INL/EXT-18-52269

Assessment of the MAMMOTH and PRONGHORN Pebble Bed Reactor Modeling Capabilities for the HTR-PM Design

Sebastian Schunert[1], Javier Ortensi[1], Ling Zou[1], Richard Martineau[1]

[1] Nuclear Science & Technology Division
Idaho National Laboratory
P.O. Box 1625
Idaho Falls, ID 83415-3840

December 2018

INL is a U.S. Department of Energy National Laboratory operated by Battelle Energy Alliance

INL/EXT-18-52269

Assessment of the MAMMOTH and PRONGHORN Pebble Bed Reactor Modeling Capabilities for the HTR-PM Design

Sebastian Schunert, Javier Ortensi, Ling Zou, Richard Martineau

December 2018

Idaho National Laboratory
Nuclear Science & Technology Division
Idaho Falls, Idaho 83415

http://www.inl.gov

Prepared for the
Office of Nuclear Regulatory Research
U. S. Nuclear Regulatory Commission
Washington, D. C. 20555
Task Order No.: NRC-HQ-60-17-T-0011

Abstract

This assessment explores the current analysis methodologies of various external and MOOSE-based tools available at the Idaho National Laboratory to model pebble-bed reactor multiphysics phenomena. The study involves three MOOSE-based, coupled codes: 1) MAMMOTH for reactor physics, 2) Rattlesnake for neutron transport and 3) Pronghorn for thermal fluids and strongly coupled conjugate heat transfer. These advanced tools are being developed under DOE-NE's Nuclear Energy Advanced Modeling and Simulation program (NEAMS). They currently contain a collection of advanced modeling capabilities that allow high-fidelity simulations of advanced reactor concepts including gas and fluoride-salt cooled pebble bed reactors. Software development of these tools follows NQA-1 standards ensuring software quality that many of the currently deployed legacy codes lack. In this work, the MAMMOTH-Pronghorn tools are compared to the legacy codes PEBBED-THERMIX-KONVEK. The external codes in use are LAMMPS for pebble mechanics and Serpent for cross section preparation. The coupling under MOOSE enables significant flexibility for modern engineering tools since MOOSE applications can be seamlessly coupled with various levels of resolution. This report focuses on low-resolution (*r*-*z*) and mid-resolution (3-D) homogenized geometries. The high-resolution Pebble Tracking Transport solution is not pursued herein and is postponed to future work. The results from this assessment show that the new MOOSE-based tools compare well with the results from legacy tools (*r*-*z*) and produce reasonable accuracy limited by the methods in the legacy tools. In the 3-D studies, the PJFNK-SPH methodology available in MAMMOTH allows the reproduction of Monte Carlo results with a transport-corrected diffusion solution. This has implications for the coupled solutions since without the SPH correction the temperature coefficient of reactivity is under-predicted and leads to lower temperature feedback and a significantly higher eigenvalue showing a difference of 2000 pcm.

Contents

1 Introduction

Any credible steady-state or transient neutronics analysis of a nuclear reactor requires solving the governing multiphysics equations simultaneously. This is particularly true for Very High Temperature Reactors (VHTRs) where large neutron migration areas and the presence of large temperature gradients strongly influence the neutron distribution in both space and energy throughout the core. For this reason, it is desirable to have a tool-set that is flexible and easily extendable in order to analyze the various physics required to model VHTRs. The MAMMOTH reactor physics and the Pronghorn thermal-hydraulics (TH) applications are ideal candidates for multiphysics modeling of VHTRs because they are built on the flexible multiphysics object-oriented simulation environment (MOOSE) and naturally provide the requisite infrastructure for multiphysics coupling.

MAMMOTH and Pronghorn are part of a set of advanced tools that are being developed under DOE-NE's Nuclear Energy Advanced Modeling and Simulation program (NEAMS). They currently contain a collection of advanced modeling capabilities that allow high-fidelity simulations of advanced reactor concept including gas and fluoride-salt cooled pebble bed reactors. Software development of these tools follows NQA-1 standards ensuring software quality that many of the currently deployed legacy codes lack.

This report focuses on assessing the current tools, MAMMOTH and Pronghorn, for multiphysics, steady-state simulations of gas-cooled pebble bed reactors (PBRs). In particular, this work aims at demonstrating existing capabilities and identify potential gaps and open questions that need to be addressed in future work-scopes. The legacy tool set PEBBED-THERMIX-COMBINE is used to establish a baseline of existing capabilities. Comparison between MAMMOTH-Pronghorn and PEBBED-THERMIX-COMBINE are performed wherever it is possible and useful to do so.

At the center of this work is the analysis of a stylized HTR-PM reactor. Exact details of reactor geometry and fuel enrichment of the actual HTR-PM are currently not available in the literature and hence missing details are chosen reasonably but not necessarily realistically. Two models are considered in this work: 1) a 2-D *r*-*z* model described in section 3.1 for comparison with the legacy tools PEBBED and THERMIX and 2) a 3-D homogenized model described in section 3.2. These models vary slightly in fuel enrichment and control rod geometry, in particular control rod volumes are not identical.

The HTR-PM is a helium-cooled High Temperature Reactor (HTR) demonstration plant currently being constructed in China and expected to start-up in 2019. The plant consists

of two nuclear steam supply systems, each featuring a power of 250MW(th); the steam supply systems are referred to as modules [1]. The scope of this analysis is limited to the nuclear core of the module and neglects the steam generator, pressure vessel, and other infrastructure that is usually considered an integral part of HTR-PM.

The HTR-PM design is loosely based on the German HTR-Module that has a rated power of 200 MW(th) [2, 3]. The main difference is a taller vessel and a larger number of pebbles in the HTR-PM. Published design specifications of the HTR-PM pertinent to this work are taken from [1] and listed in Table 4. Important design information is not available, including total height of the vat (cavity height), dimensions of the exit chute, dimensions of the axial reflectors, distance and design specifications of the control rods, biological shield (carbon bricks) and details about the graphite used in the various core structures. These design details are chosen as reasonably as possible. However, we stress again that the goal of this work is not to create an accurate HTR-PM model but to demonstrate existing capabilities and to expose capability gaps in the current tools.

Table 1: Design data of HTR-PM partially published in [1].

Parameter	Value	Unit
Published specifications		
Reactor thermal power	250	MW(th)
Primary helium pressure	7	MPa
Inlet temperature	250	°C
Outlet temperature	750	°C
Core diameter	3	m
Number of pebbles	420,000	
Equivalent core height	11	m
Added specifications		
Exit chute radius	0.25	m
Exit chute height	2.906	m
Cone height	0.7105	m

The axial symmetric cylindrical geometry model (termed *r*-*z* model) is used for comparing MAMMOTH/Pronghorn with PEBBED-THERMIX results. The dimensions and makeup of this *r*-*z* model are depicted in Fig. 1. It consists of 9 distinct material regions: pebble bed core (1), carbon brick (2), bottom, side, and top reflectors (3-5), top cavity (6), control rod inserted (7), empty control channels (8), and riser (9). The dimensions of the regions

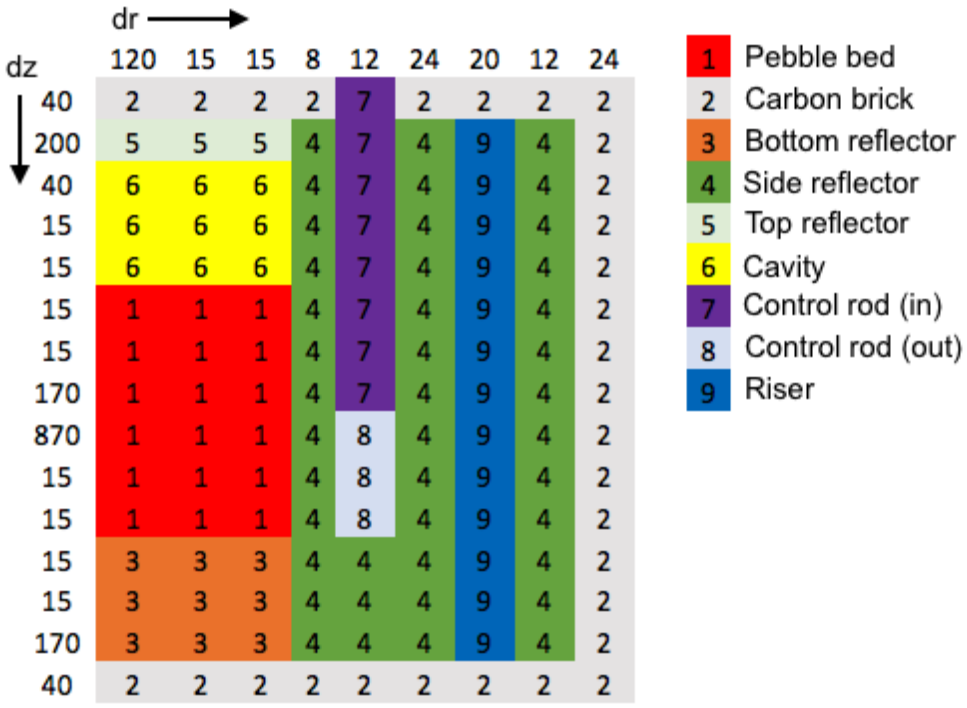

Figure 1: Geometry of the *r*-*z* model of HTR-PM.

are indicated as interval width on the top and left side. We note that in particular the following approximations: the top cone is not modeled, the bottom cone and exit chute is not modeled, and the feeding pipe is not modeled.

2 Computer Codes

2.1 PEBBED-THERMIX-COMBINE

PEBBED-THERMIX-COMBINE is a legacy research tool developed at INL for multi-physics PBR k-eigenvalue and fuel cycle analysis. It is comprised of several modules: the PEBBED code [4–6], the THERMIX-KONVEK code [7], and the COMBINE code [8]. PEBBED acts as control module for the three codes. The modules are responsible for neutronics, TH, and cross section preparation within the PEBBED-THERMIX-COMBINE system, respectively.

PEBBED is a reactor physics code designed to directly solve for the asymptotic burnup state of PBRs. To this end, it solves the neutron diffusion equation coupled with the transmutation and pebble circulation equations. The neutron diffusion equation is discretized using the Finite-Difference method on a one-, two-, or three-dimensional orthogonal mesh, i.e. element boundaries always intersect at right angles; two Coordinate systems, Cartesian and Cylindrical are available. Details of the discretization scheme are omitted here because it is rather standard and fully described in Ref. [4]; the original text describing this discretization scheme is [9]. Within this work, we solve the k-eigenvalue problem with TH feedback for a fresh core. Therefore, the transmutation equations and their coupling to the pebble circulation equations are not discussed. PEBBED solves the few-group diffusion equation, where the number of groups is typically smaller than 10. Few-group cross sections are provided to PEBBED as cross-section input file, labeled the *default cross section set* and then potentially recomputed by COMBINE during the calculation sequence, or directly in the PEBBED standard input file.

THERMIX-KONVEK is a TH code for PBR analysis that is part of the V.S.O.P. package (Very Superior Old Programs) [7]. THERMIX-KONVEK is limited to *r-z* geometry. The relevant source code is ported into PEBBED-THERMIX-COMBINE and PEBBED calls THERMIX-KONVEK as a subroutine. PEBBED and THERMIX-KONVEK share a common mesh thus limiting PEBBED to *r-z* geometry as well when executing coupled calculations. Besides the shared portion of the mesh, THERMIX-KONVEK supports additional regions *outside* the PEBBED mesh to describe features deemed unimportant for neutronics modeling. PEBBED and THERMIX communicate through the power density passed from PEBBED to THERMIX, and the solid temperatures averaged over spectral zones passed from THERMIX to PEBBED.

THERMIX-KONVEK computes temperature and flow conditions in the pebble bed and the surrounding graphite reflector. It solves for pressure, velocities, gas temperature, and solid temperature as primary variables. Flow field calculations including all but the solid temperature variable are performed by KONVEK, while the THERMIX main routine computes the distribution of solid temperatures. The calculation of the variables is decoupled within a nested iteration strategy depicted in Fig. 2. First, KONVEK solves for the pressure and the flow field, then updates the gas temperature and finally the solid temperature distribution; each set of equations and in addition the KONVEK set (pressure, flow field, and gas temperature) are iterated to convergence before advancing to the next subset of equations.

KONVEK solves a legacy set of equations described in detail in [7]. It consists of quasi-static conservation of mass, momentum, and fluid energy, i.e. time derivatives are neglected in all equations. In addition, the advection terms in the momentum equations are neglected and the frictional forces are represented by a constitutive law. THERMIX solves the transient energy conservation equation in a solid medium. THERMIX and KONVEK interact via convective heat transfer terms in the fluid and solid energy equations.

COMBINE generates few-group cross sections for PEBBED from a 167 fine-group cross section library prepared with Los Alamos' NJOY code [10]. To this end, it solves B-1 or B-3 equations in 167-groups, Bondarenko's self-shielding method with Dancoff-Ginsburg correction are used for self-shielding; optionally Nordheim's self-shielding method is available for resolved resonances. The self-shielding of thermal cross sections is modeled using the the Amouyal/Benoist/Horowitz (ABH) method. COMBINE accounts for double heterogeneity (TRISO particles in pebbles) of cross sections by using escape probabilities computed by Stamatelatos and LaBauve's method [11]. COMBINE also packages the ANISN [12] code for performing one-dimensional transport calculations for including reactor leakage effects on local spectra.

2.2 LAMMPS

LAMMPS is the Large-scale Atomic/Molecular Massively Parallel Simulator developed at Sandia National Laboratory [13, 14]. LAMMPS' role in this work is to provide the position of each pebble in the PBR core. The point cloud of pebble locations is required by Serpent for cross section computation.

LAMMPS is originally developed to solve molecular dynamics problems for material science applications by solving the many-body equations of motions with arbitrary inter-

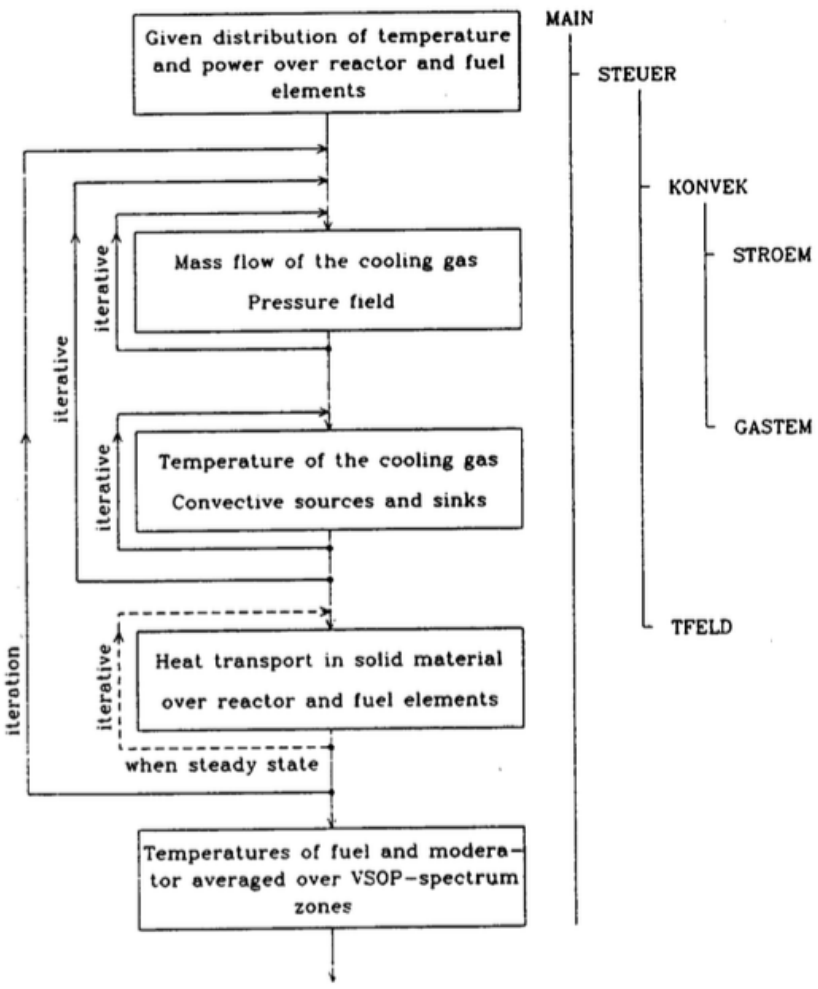

Figure 2: THERMIX iteration scheme; picture courtesy [7].

particle potentials. LAMMPS' *granular* package [15] allows the simulation of elastic solid bodies that only exert forces on each other when in physical contact; the granular package provides Hookean and Hertzian force models. In contrast, typical material science applications feature long-distance potentials that smoothly limit to zero as the inter-particle distance increases. Codes simulating granular materials are often referred to as Discrete Element Method (DEM) as opposed to Molecular Dynamics (MD) codes.

LAMMPS is used for PBR simulation by Rycroft [16] motivating the deployment within this project. It replaces the PEBBLES DEM code [17] used for the completion of the

previous HTR-10 study [18]. The necessity for replacement arises from two short-comings of PEBBLES: first, PEBBLES is multi-threaded but not parallelized limiting its parallel scalability, second, PEBBLES is not actively maintained and version controlled and does not follow a software quality assurance plan. PBRs of the 250 MW(th) range, such as HTR-PM, HTR-Module, or Xe-100, contain about 400,000 pebbles in the core region. PEBBLES requires in excess of four weeks to compute the pebble locations for a circulated bed using 32 threads, while LAMMPS can solve the same problem in less than 24 hours on 432 CPUs. The execution time of PEBBLES is deemed unacceptably long for our PBR analysis needs.

2.3 Serpent

Serpent [19] is a three-dimensional continuous-energy Monte Carlo reactor physics code developed at VTT Technical Research Centre of Finland. It is selected as the main cross section preparation tool for this project because it offers 3-D spatial homogenization and group constant generation for deterministic reactor simulator calculations. At the same time, Serpent 2 provides a detailed reference calculation without energy, angular, or spatial discretization error. The version used in this work is 2.1.28.

Serpent has unique capabilities with regard to the modeling of PBRs. Serpent cannot only model the random pebble distribution, but, in addition, it can model the random TRIstructural-ISOtropic (TRISO) distribution inside the pebbles. Serpent only requires a file with the position of each pebble's center point, much like the output generated by LAMMPS. Serpent uses this information to explicitly represent the location of pebbles in the core without applying any homogenization.

Serpent has been used at the INL to prepare neutron cross sections since 2010 [20]. Recent work with modeling and simulation of the TREAT and HTR-10 reactors [18, 21, 22] has improved the process for the preparation and tabulation of multi-group cross sections from Serpent to the MAMMOTH reactor physics application, thus making it a compelling candidate for this task.

2.4 PRONGHORN

Pronghorn is a MOOSE-based TH code that solves equations of fluid mechanics, heat transfer, and heat conduction for problems where the complicated geometry and interaction of fluid and solid is treated in an average sense via appropriate correlations [23–25]. Currently, Pronghorn is equipped with equations and correlations to describe the flow and heat-transfer in PBRs. The distinct difference between Pronghorn and computational fluid dynamics codes is that the geometry of the pebble bed is not represented exactly, i.e. as a collection of pores formed by a collection of pebbles. Instead, effective porosity, heat transfer coefficients, and pressure loss correlations are used to describe the interaction of fluid and solid.

Pronghorn can solve both legacy and modern, compressible Euler type equations sets. The legacy equations are similar to the equations THERMIX-KONVEK solves with the exception that Pronghorn can include time derivative terms in the mass and momentum conservation equations. The momentum conservation equation is usually solved for velocities and substituted into the mass conservation equation leading to the pressure-Poisson form of the legacy equation set.

Pronghorn discretizes the legacy equation using MOOSE's continuous finite element method (CFEM) [26]. CFEM requires stabilization if the element Peclet number exceeds unity. Pronghorn implements a mixed finite element method described in Ref. [27] to ensure stability at large element Peclet numbers [24].

Pronghorn features an array of advanced capabilities that are not implemented in THERMIX-KONVEK. First, conjugate heat transfer can be taken into account using the *interface kernel* system. Pronghorn results with and without conjugate heat transfer are included in this report. Second, Pronghorn can model spatially dependent porosities computed by LAMMPS, and finally, Pronghorn implements a modern equation system allowing for a significantly more accurate representation of flow conditions outside the pebble bed. With the exception of conjugate heat transfer, the advanced features of Pronghorn are not exercised in this work for two reasons:

- The focus of this work is the coupling of neutronics and thermal-hydraulics and not the creation of a high-fidelity HTR model.
- The legacy code suite PEBBED-THERMIX-COMBINE does not implement any of these advanced features.

Future work will bring the advanced features to bear on more realistic PBR models and demonstrate their accuracy and efficiency.

2.5 MAMMOTH/Rattlesnake

The main focus of this work is to demonstrate the ability to perform coupled neutronics/thermal-hydraulics (N/TH), steady-state PBR calculations with MAMMOTH and Pronghorn and compare them with results obtained from legacy codes. Within the MOOSE [26] herd, Rattlesnake and MAMMOTH are the designated neutronics and reactor physics applications, respectively, while Pronghorn solves equations pertinent to TH of PBRs. The relevant steady-state physics of neutronics is described by the neutron transport equation in its k-eigenvalue form. In this report we omit stating the transport equation and refer the reader to Ref. [28] for a thorough discussion. It it sufficient to say that the neutron transport equation requires cross sections describing the interaction of neutrons with fuel, moderator and structural material in the reactor core. MAMMOTH is ultimately responsible for computing the core eigenvalue and power density. The power density drives the heat generation rate that accounts for the main interaction with TH.

MAMMOTH is based on MOOSE [26], a finite element method framework that focuses on multiphysics simulations with fully or tightly coupled physics applications. In addition to implementing reactor physics specific capabilities such as depletion and equivalence methods, MAMMOTH seamlessly interfaces with several other MOOSE applications including Rattlesnake [29] for radiation transport algorithms, MOOSE modules for heat transfer and solid mechanics [26], BISON [30] for fuel performance modeling and Pronghorn [23–25] for thermal fluids calculations in PBRs. The Rattlesnake neutron transport solver incorporates a variety of spatial and angular discretization methods including diffusion, P_N and S_N (both 1^{st} and 2^{nd} order formulations). In this work, we exclusively use the continuous FEM diffusion solver. In addition, the computation of directional diffusion coefficients requires the solution of a neutron-transport like equation that is facilitated with the first order S_N solver. A detailed discussion of the available transport discretization options in Rattlesnake can be found in Ref. [28].

PBRs feature a cavity above the top-cone of the reactor that often serves as entry point of the Helium coolant into the pebble bed. Neutronically, this region is optically transparent supporting significant streaming and a very small probability of collisions for neutrons traversing it. This traditionally poses problems for obtaining diffusion coefficients because the validity of the classical diffusion approximation for neutron transport applications ulti-

mately requires short mean free paths and many scattering collisions before absorption; this is evident in the standard definition of the diffusion coefficient as the inverse of three times the transport cross section [31]. For optically thin regions, the diffusion coefficient tends to infinity. A variety of methods exists to meaningfully define diffusion coefficients in near-void regions, e.g. Morel's non-local diffusion coefficients [32] that are successfully used by Trahan [33] for analysis of reactors with optically thin channels, Monte-Carlo methods have been equipped with tallies to compute diagonal tensor diffusion coefficients based on the cumulative migration method [34]. Serpent currently does not include the capability to generate anisotropic diffusion coefficients in extended geometries to allow better modeling of neutron streaming effects within the diffusion approximation and hence we resort to using Morel's non-local diffusion coefficient in the top core cavity.

The computation of non-local diffusion tensors was implemented in the Rattlesnake transport solver [22, 33] to address the streaming effects through the region above the pebble bed. In addition to computing tensor diffusion coefficients, an advanced implementation of the traditional equivalence procedure [35] developed at INL, the PJFNK-SPH [36, 37], is employed to ensure preservation of the reaction rates between the reference Monte Carlo model and the cross section set used in the MAMMOTH model.

For the deterministic transport model, we do not explicitly model the location of all pebbles separately even though this capability is available in MAMMOTH through the pebble tracking transport algorithm implemented in Rattlesnake [38]. Instead, we infer the outline of the cylindrical core region and the top cone from the point cloud provided by LAMMPS and homogenize the top core cavity and the upper cone between $z_{c,1}$ and $z_{c,2}$ where $z_{c,1}$ and $z_{c,2}$ are the z-coordinates of the lower onset of the top cone and the cone's tip. Throughout this work, the MAMMOTH geometry is homogenized and neutronics is represented by the diffusion model.

2.6 MAMMOTH/Pronghorn Coupling

MAMMOTH and Pronghorn are both built on the MOOSE framework and hence can naturally be coupled. MOOSE provides two approaches to coupling different multiphysics equation sets: first, full coupling solves all equations concurrently in a single nonlinear system, and second, tight coupling deploys a Picard iteration scheme. Picard iterations partition the variables into groups and solve the equations pertaining to each group separately, then communicating updated values of the variables to the next group of equations to be solved. Full coupling is the method of choice if the problems are discretized on the

same mesh, while Picard iterations are typically preferred if the time or length scales of the problems differ significantly. In this work, both fully and tightly coupled schemes are exercised.

The sets of neutronics and TH equations are coupled through the graphite temperature and power density. Graphite temperatures are computed by Pronghorn and provides feedback to the cross sections appearing as parameters in the neutronics equations, while power density is computed from the fission density by Rattlesnake. It appears as source term in the graphite heat conduction equation.

3 Analysis Methodology

3.1 Two-dimensional *r-z* Analysis Methodology

The two-dimensional, cylindrical geometry model is a low fidelity model that is created for comparison of MAMMOTH-Pronghorn with the legacy code suite PEBBED-THERMIX-COMBINE. Comparison of stand-alone neutronics and TH results is performed. Comparison of coupled neutronics/thermal-hydraulics models was not completed due to shortcomings in PEBBED's cross section preparation capabilities.

3.1.1 Neutronics Models

PEBBED is used to create a constant cross section set for each of the nine regions of the R-Z model depicted in Fig. 1. The cross section set is processed into MAMMOTH's input cross section format so that the cross sections used by PEBBED and MAMMOTH are identical.

PEBBED assigns separate cross section sets to each macro-element, where each macro-element is defined as a collection of mesh-elements that form a right quadrilateral. Each of the separate identifiers in the *r-z* geometry depicted in Fig. 1 is a macro-element. In the absence of cross section updates by COMBINE, cross sections in macro-elements are identical as long as the region identifier is the same. In MAMMOTH, cross sections can be assigned by *blocks* or *material ids*. *Blocks* are a collection of mesh elements but are not necessarily quadrilateral in shape, and *material ids* are an integer number assigned to each mesh element indicating the cross section set assigned to this element.

Both MAMMOTH and PEBBED discretize the problem with orthogonal quadrilaterals. The initial MAMMOTH mesh has 11 radial and 46 axial mesh subdivisions resulting in 506 elements; the mesh is chosen to limit element width to roughly 40 cm. The initial PEBBED mesh 14×86 elements resulting in $1,204$ elements; the PEBBED mesh is chosen to limit element width to 20 cm except for the axial spacing in the reflector regions. The finer PEBBED mesh is necessary because the numerical method represents the flux as constant across elements while MAMMOTH's FEM method represents the flux as piecewise linear function.

A sequence of five and six refinement steps is considered for MAMMOTH and PEBBED,

respectively. These refinement levels are referred to as r$< n >$ and p$< m >$ for MAMMOTH and PEBBED respectively, with $n = 0, ..., 4$ and $m = 0, ..., 5$. In this study, we apply uniform refinement for the MAMMOTH model which subdivides each element into four quadrilaterals. PEBBED refinement is limited by the total number of subdivisions per axis due to using static arrays. Therefore, PEBBED requires a more judicious choice of local mesh refinement. The number of elements for MAMMOTH and PEBBED for each mesh refinement level and is shown in Table 2. The mesh refinement strategy in PEBBED is detailed in Table 2's fifth column. The finest meshes have an average radial and axial mesh spacing of $\Delta h_r = 1.4$ and $\Delta h_a = 2.2$, and $\Delta h_r = 2.6$ and $\Delta h_a = 7.2$ cm for MAMMOTH and PEBBED, respectively. For both MAMMOTH and PEBBED, radial mesh spacing is selected to be smaller, because of the smaller radial extent of the core and the resulting steeper flux gradient.

Table 2: Mesh refinement levels and number of elements for MAMMOTH and PEBBED for the neutronics without thermal feedback study. For PEBBED, the mesh refinement strategy for each step is summarized in the fifth column.

MAMMOTH		PEBBED		
r0	506	p0	1,204	$\Delta h < 20$ cm (except axial reflector)
r1	2,024	p1	3,538	$\Delta h_r < 10$ cm, refine axial reflector $\Delta h_a < 20$ cm
r2	8,096	p2	10,679	ensure $\Delta h_r < 5$, $\Delta h_a < 10$ cm
r3	32,384	p3	15,385	refine radially
r4	129,536	p4	18,128	CR & high error
		p5	23,040	CR & high error

3.1.2 Thermal-Hydraulics Models

THERMIX and KONVEK require separate assignment of regions to each macro mesh element; the regions indicate if fluid flow occurs, how it interacts with the solid heat conduction, and what material properties are used. The region assignment for the THERMIX-KONVEK model is presented in Fig. 3. We discuss the different THERMIX and KONVEK regions separately.

The THERMIX model has only four distinct regions:

- The pebble bed region is a *solid material zone* allowing exchange of heat with the fluid field and has a packing fraction of 0.61.
- The cavity is a *solid material zone* allowing exchange of heat with the fluid with a packing fraction of 0.
- The graphite is a *solid material zone* that does not allow exchange of heat with the fluid. It has a packing fraction of 1.
- The BC regions are *fluid zones* that allow imposition of boundary conditions.

Boundary conditions in THERMIX are applied by adding an additional layer of *fluid zones* around the circumference of the model. The additional macro-element is assigned a heat transfer coefficient and an ambient temperature. By setting the heat transfer coefficient to a very large number, 10^8 in our case, Dirichlet boundary conditions are emulated. The temperature is fixed at 523 K. The heat conductivity in the graphite is fixed at $26\frac{\mathrm{W}}{\mathrm{K\,m}}$, while the heat conductivity in the pebble bed is computed internally using the Zehner-Bauer-Schluender correlation (ZBS) [7, 23].

The KONVEK model comprises eight regions:

- The pebble bed is a *pebble bed* zone and the only region for which a convective heat source is computed. It has a porosity of 0.39.
- The cavity and riser are vertical pipes (VP) with porosity 1.
- The lower and upper plenum and the Helium source are horizontal voids (HV). A mass flow rate of 96 kg /s enters the model in region 9 and is collected and removed in region 8. All horizontal voids have porosity 1.
- The flow equations are not solved on *no flow zones* (id 4) and *excluded* (id 0) zones.

KONVEK's system pressure is set to 7 MPa.

The Pronghorn porous fluid model is constructed to be as close to the THERMIX-KONVEK model as possible. The reactor is divided into three distinct sections: the pebble bed, the cavity, and the reflector. The dimensions of these regions are identical to the respective regions in Fig. 3 with the difference that regions 19, 20, 21 are absent in the Pronghorn model.

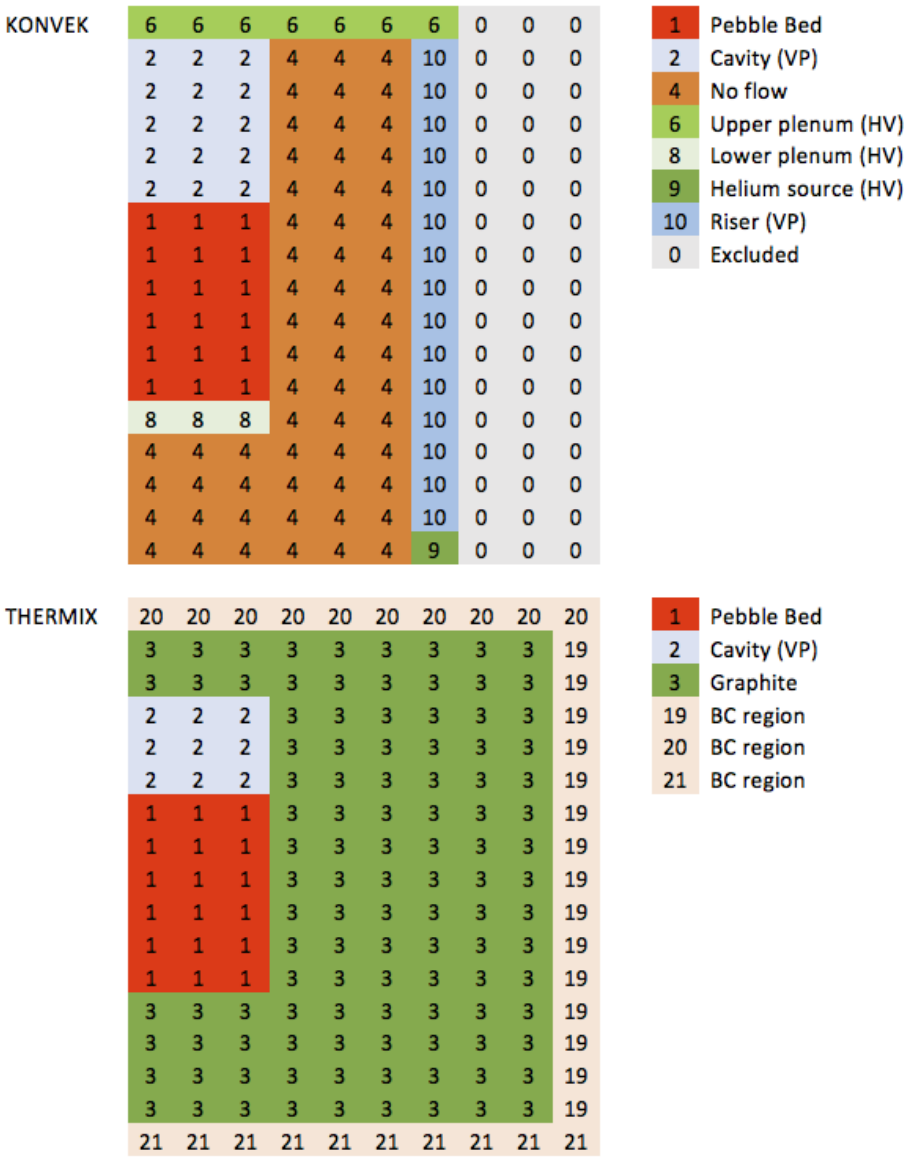

Figure 3: Region assignment in the THERMIX-KONVEK *r-z* model.

The reflector is uniform and assumed to only consist of graphite with a thermal conductivity of $26\frac{\mathrm{W}}{\mathrm{K\,m}}$. Only solid heat conduction equations are solved in the reflector region and Dirichlet boundary conditions with a value of 523 K are applied on the outer boundary.

Flow enters through a sideset located on top of the cavity with a uniform vertical velocity of 5.4 $\mathrm{m/s}$ and a temperature of 523 K and exits through the bottom of the pebble bed. Appropriate boundary conditions are applied on sidesets above the cavity, below the core, and around the cavity and core. These boundary conditions are tabulated in Table 3. The cavity has a porosity of 1 and constant drag coefficients are computed using a Darcy coefficient of 10 and a Forchheimer coefficient of 1. The core has a porosity of 0.39 and KTA drag coefficients are used. Details pertaining to these correlations can be found in Ref. [23].

Table 3: Boundary conditions for Pronghorn model.

Equation	Above cavity	Below Pebble bed	Circumference
Fluid Energy	Dirichlet $T_f = 523$ K	natural	natural
Pressure Poisson	Inflow $\rho v_z = -13.7\frac{\mathrm{kg}}{\mathrm{sm^2}}$	Outflow $p = 7$ MPa	natural
Momentum (r)	natural	natural	solid wall $\rho v_r = 0$
Momentum (z)	natural	natural	natural

3.2 3-D Analysis Methodology

The 3-D analysis methodology is depicted in Figure 4. The work-flow starts with the determination of the pebble positions via the LAMMPS simulation. The LAMMPS output is then processed with a set of Python scripts that assign the pebble type to each computed pebble location randomly in such a way as to preserve the total number of each pebble type. The output of this python script is a pebble distribution file that is included in Serpent during the generation of the base model. The next step entails the preparation of the Constructive Solid Geometry (CSG) input for the homogenized domain used in the 3-D MAMMOTH simulation. A Python meshing framework that accesses the CUBIT API processes the input CSG directives and generates both an Exodus II mesh file and a Serpent homogenization file. This latter file is included in the preparation of the final Serpent model that is used to generate homogenized cross sections and group-wise fluxes for SPH calculations.

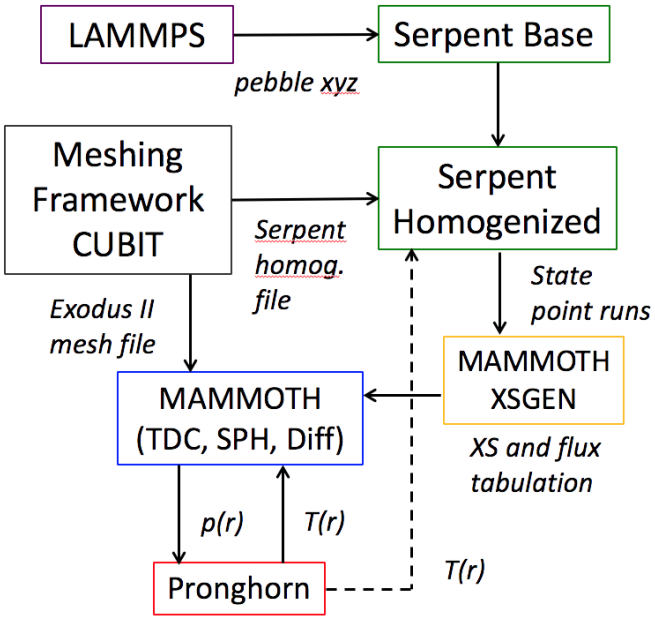

Figure 4: Analysis work-flow for the 3-D HTR-PM.

A set of state-point calculations with the Serpent model generate the cross sections and tally output files for the full domain. Each state-point corresponds to a different combination of values of the state variables that parameterize the nuclear cross sections. The MAMMOTH cross section post-processor, XSGEN, compiles the tabulations and generates the YAKXS formatted file. The exodus mesh and the YAKXS file are used in the preparation of the MAMMOTH/Rattlesnake input. MAMMOTH/Rattlesnake TDC and SPH calculations prepare the final tensor diffusion coefficients in void regions and SPH factor tabulation. Finally, the models are ready for the multi-physics simulations based for SPH-corrected diffusion with tensor diffusion coefficients.

For computing accurate cross sections in VHTR, it is imperative to account for multiphysics conditions during the cross section preparation step [39]. This can be accomplished by providing a sufficiently accurate temperature distributions to Serpent. As the temperature distribution is not initially known, an iterative procedure can be used that is illustrated in Fig. 5.

The data preparation starts by estimating the average temperature of the reflector as a function of the core average temperature using PRONGHORN. The power distribution is only

roughly estimated by solving the neutronics problem with an existing cross section library. In this work we use the standard PEBBED cross section library. For various power levels, we determine the core average and reflector average temperatures. The reflector is split into three regions, top, side and bottom reflector. For each power level we determine the average pebble bed temperature and the correlated averaged temperature for each reflector region. For a selected isothermal core temperature, the average temperatures of the reflector are interpolated from these results allowing the Serpent calculation to account for reflector temperature effects on the fuel cross sections.

The main stage of the cross section computation is comprised of Serpent cross section calculations, tensor diffusion coefficient calculations, equivalence calculations, tabulation, and finally coupled neutronics/thermo-hydraulics calculations. In the first traversal isothermal core and reflector temperatures are assumed to be constant. For a given core temperature, reflector temperatures are computed using the table created in the bootstrapping stage. Later iterations have updated temperature fields available. After solving the coupled N/TH stage, the iterative procedure may be repeated. In this work, we do not update temperatures for cross sections because we lack a reference solution to compare results to.

We point out that the outlined process is necessary due to a lack of a native online cross section generation capability in MAMMOTH. In the future, we plan to abandon this iterative approach in favor of an inline cross section processing that is more suitable for multiphysics modeling of VHTRs.

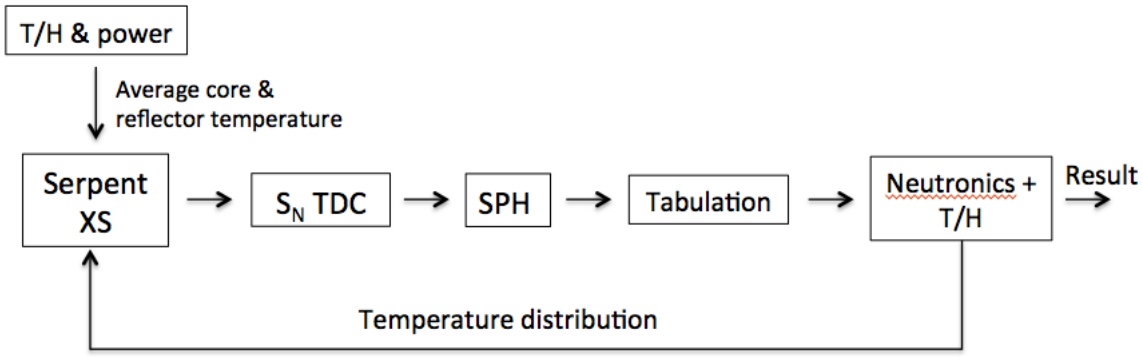

Figure 5: Cross section preparation sequence for HTR-PM.

3.2.1 The Serpent Model

The high-resolution Serpent model is consistent with the dimensions introduced in Figure 1. In addition, this model explicitly represents the pebbles, control rods, KLAK orifices and helium channels present in the HTR-PM design. Table 4 lists the specifications used in the Serpent model and corresponding references. Note that the diameter of the helium coolant channel is approximated and the number of control rods and KLAK orifices might have changed in the latest design iterations [40].

The active core region contains both fueled and dummy pebbles. The fuel pebbles include explicit, randomized TRISO particles inside the pebble fueled region, whereas the dummy pebbles are made entirely of graphite. The dimensions and compositions of the various TRISO layers are based on [41]. The top, bottom and side reflector compositions originate from [42]. The control rods are positioned in a non-symmetric pattern [43] and the control rod specifications are the same provided in [42].

Figures 6 and 7 depict the final Serpent model and show the surfaces used to delineate the flux tally regions. Note that the bottom reflector in the Serpent model extends 3.65 m below the cylindrical portion of the pebble-bed. There are a total of 31 unique cross section regions and 6,498 flux tally regions. The cross sections and fluxes are condensed to the coarse 4 energy group structure presented in Table 5.

Table 4: Specifications for the HTR-PM Serpent Model

Parameter	Value	Unit	Source
Active Core Region			
Enrichment of fresh fuel pebbles	4.1	%	[44]
Uranium loading per pebble	7.0	g	[44]
Diameter of the fuel pebbles	6.0	cm	[1]
Diameter of the fueled region in a pebble	5.0	cm	[1]
Average number of particles per pebble	11,593		
Number of pebbles	420,000	-	[44]
Fraction of fueled pebbles in the core	7/15	-	[44]
Reflector Region			
Number of control rods	8	-	[1]
Control rod hole diameter	12	cm	[42]
Control rod hole radial position	164.0	cm	Fig. 1
Number of KLAK channels	22	-	[1]
KLAK orifice diameter	10.6	cm	[42]
KLAK radial position	164.0	cm	Fig. 1
Number of helium coolant channels	30	-	[1]
Helium coolant channel diameter	15.0	cm	[approx.]
Helium coolant channel radial position	204.0	cm	Fig. 1

Table 5: Upper energy group boundaries (eV) used in Fort St. Vrain calculations [45].

Energy group	Upper boundary [eV]
4	2.38
3	1.76E1
2	1.83E5
1	40E6

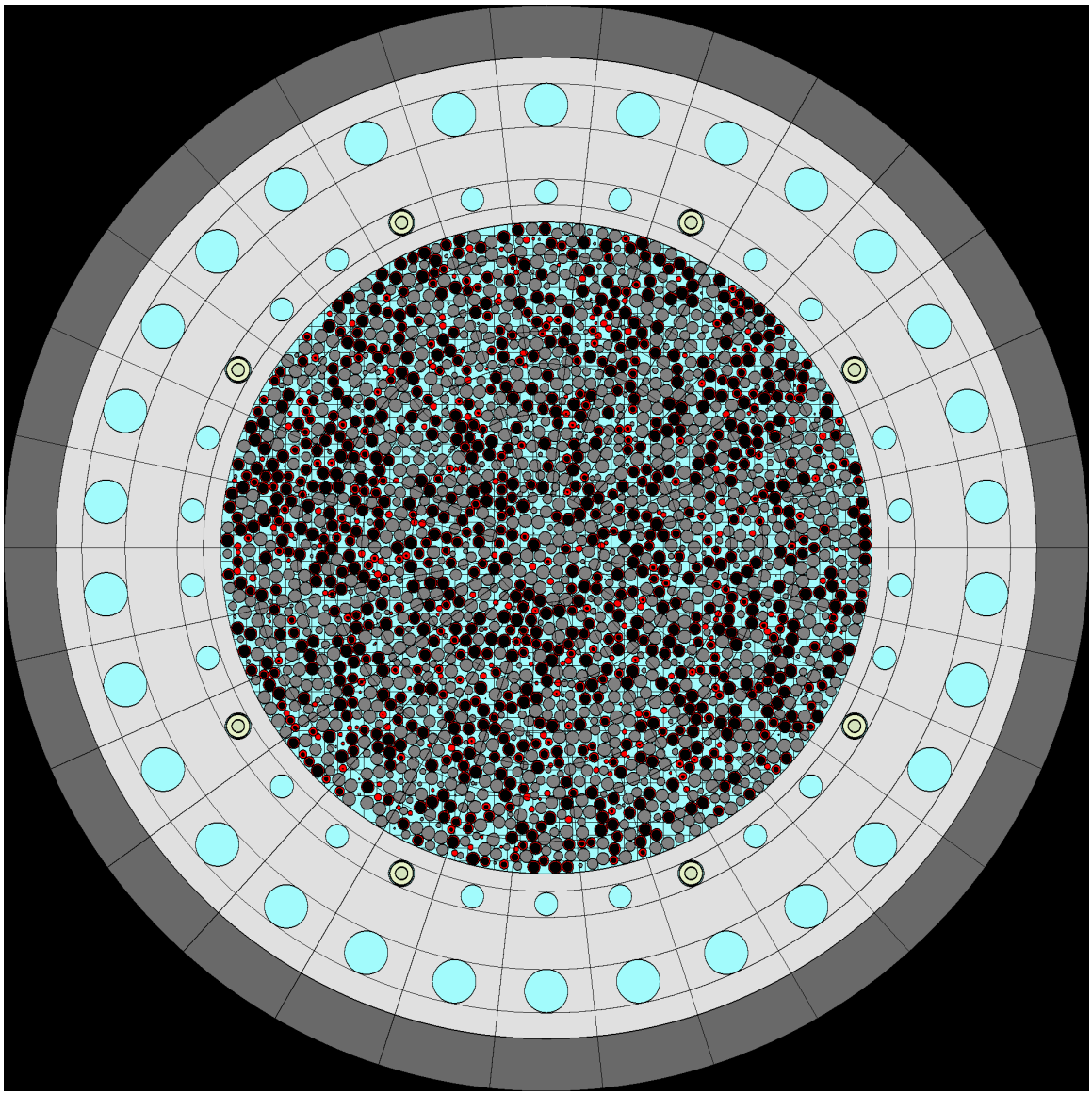

Figure 6: Serpent model showing flux tally regions (X-Y).

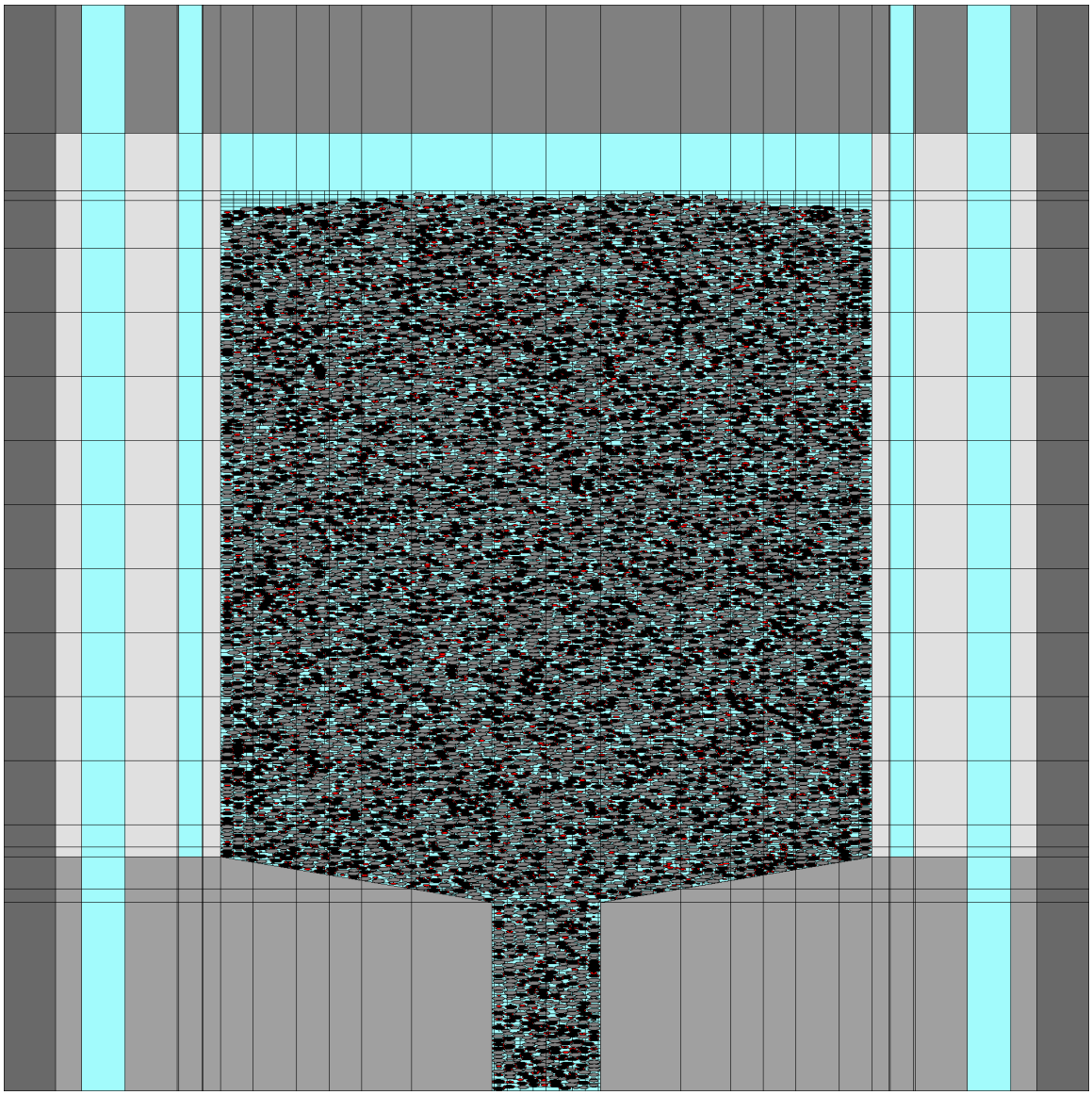

Figure 7: Serpent model showing flux tally regions (X-Z).

The state-points shown in Table 6 are used in the preparation of the cross section and flux tabulations. The values are based on preliminary PEBBED-THERMIX calculations at various power levels. The average pebble temperature applies to both fuel and dummy pebbles. Only this solid temperature in the pebble-bed (T_{solid}) is considered in the feedback tables for the model. The complexity of the feedback model can be easily extended in the future by increasing the model resolution (i.e. calculating a fuel temperature) and running more tabulation cases (i.e. $\Sigma_{x,g}(T_{fuel}, T_{moderator}, T_{reflector})$).

Table 6: State-points used in the tabulations of the solid temperatures $[K]$

case	average pebble (T_{solid})	average top reflector	average side reflector	average bottom reflector
1	500.0	524.0	526.0	527.0
2	700.0	524.0	579.0	600.0
3	900.0	524.0	579.0	600.0
4	1100.0	524.0	579.0	600.0
5	1300.0	524.0	579.0	600.0

3.2.2 The MAMMOTH Model

The MAMMOTH mesh is shown in Figure 8. The mesh includes 54,656 elements. The final model extends 2.5 m in the radial direction and 14.8 m in the axial direction. The bottom reflector is 1.5 m tall and includes three axial regions to model the bottom cone and chute. The top cone created by the pebbles and the upper void region above the core are resolved with the axial and radial regions currently defined. The top reflector extends for 2 m, the borated bricks located above and below the reflectors are not modeled and replaced by vacuum boundary conditions. The control rod position matches that of the Serpent model at 11 m measured from the bottom of this model.

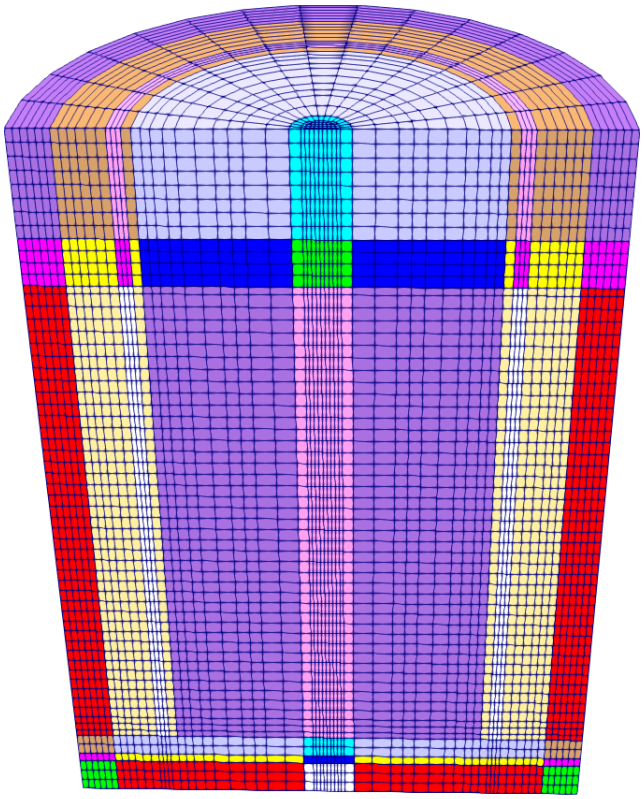

Figure 8: Mammoth 3-D mesh.

3.2.3 The Pronghorn Model

Pronghorn uses the same mesh as MAMMOTH for solving the relevant TH equations. The Pronghorn model is comprised of three different regions: pebble bed, cavity, and graphite. The structure in the reflector and cone regions that is accurately represented in the Serpent and MAMMOTH neutronics model is simplified to a homogeneous graphite region. The pebble bed and cavity are the cylindrical regions of radius up to 1.5 m and elevations between elevations of 1.5 m and 11.9 m and 11.9 m and 12.8 m, respectively.

The Pronghorn model is a straight-forward extension of the *r*-*z* model to a three-dimensional geometry. Fluid flow is solved only in the cavity and pebble bed regions. Pebble bed and cavity are separated from the surrounding reflector by three side-sets arranged on top of the cavity, at the core outlet, and at the perimeter of the cavity/pebble bed. Fluid flow is

introduced at the top sideset and vanishes at the bottom sideset which is prescribed by the applied boundary conditions that are identical to those deployed on the *r-z* model in Table 3.

In contrast to the *r-z* model, the thermal conductivity is not fixed but temperature dependent. We use the graphite properties of the Sigri Al 2-500 electric graphite pebbles used in the SANA benchmark provided by Pronghorn [23]. We exercise Pronghorn's ability to model conjugate heat transfer via the *interface kernel system* and discuss the impact on the computed solution.

The described TH model is designed to facilitate a proof of principle of MAMMOTH-Pronghorn coupling. It should not be considered a physically realistic model of the HTR-PM code because it neglects the following important physical mechanisms:

- Cooling of reflector by Helium in the riser.
- Cooling of the pebbles in the lower cone, cooling of the cone itself, and heating of the coolant.
- Effect of the cone region on the fluid flow field.

While these physical mechanisms are important for a realistic HTR-PM model, they have negligible implications for the process of coupling MAMMOTH and Pronghorn.

4 Results

4.1 Comparison to Legacy Codes

This section compares results from the legacy tools PEBBED-THERMIX-COMBINE with MAMMOTH-Pronghorn. First, we compare results obtained without TH feedback in section 4.1.1, in section 4.1.2 we compare key thermal-fluids quantities obtained using a power distribution computed in section 4.1.1, and finally we discuss coupled steady-state solutions in section 4.1.3. Throughout this section, the cylindrical (r-z) model is used exclusively because PEBBED-THERMIX-COMBINE is limited to cylindrical geometry.

4.1.1 Stand-Alone Neutronics

In this section, we compare results obtained with PEBBED and MAMMOTH without thermal feedback. We use the same cross sections, geometry, and boundary conditions in both codes but MAMMOTH and PEBBED discretize the diffusion equation differently. We compare the computed eigenvalues and power distributions.

The eigenvalues computed with MAMMOTH and PEBBED agree well with each other and converge to the same value as the mesh is refined. In Table 7, eigenvalues of MAMMOTH and PEBBED are listed vertically and horizontally, respectively. The difference of a pair of eigenvalues in units of pcm,

$$\frac{\Delta k}{k} = 1 \times 10^5 \frac{(k_{\text{PEBBED}} - k_{\text{MAMMOTH}})}{k_{\text{MAMMOTH}}} \tag{1}$$

is given at the intersection of the corresponding row and column number. We observe diminishing differences in eigenvalues with increased mesh refinement. The difference between the last two eigenvalues computed by MAMMOTH show a difference of only 3 pcm, while PEBBED's eigenvalue still varies by 9 pcm. Therefore, a finer PEBBED mesh is required to improve agreement with MAMMOTH; however, further refinement is precluded by the fixed size of PEBBED's static arrays. The most converged eigenvalues are in excellent agreement with a difference of only 21 pcm.

Power densities computed by MAMMOTH and PEBBED converge to the same limit almost everywhere except for a small region, potentially of measure zero, at the top of the pebble bed.

Table 7: Comparison of eigenvalues computed with PEBBED and Rattlesnake for various mesh refinement levels. The difference of a combination of Rattlesnake and PEBBED eigenvalues is given in units of pcm.

		Refinement → PEBBED					
		p0 1.08207	p1 1.08113	p2 1.08097	p3 1.08103	p4 1.08078	p5 1.08069
MAMMOTH		Eigenvalue difference [pcm]					
r0	1.08002	190	103	88	94	70	62
r1	1.08029	165	78	63	69	45	37
r2	1.08038	156	69	55	60	37	29
r3	1.08043	152	65	50	56	32	24
r4	1.08046	149	62	47	53	30	21

For measuring the difference of power densities, we compute the relative difference of MAMMOTH and PEBBED computed results:

$$\Delta p(\vec{r}) = 1 - \frac{p_M(\vec{r})}{p_P(\vec{r})}, \tag{2}$$

where p_M is MAMMOTH's power density and p_P is PEBBED's power density. We quantify the discrepancy using the minimum and maximum value and RMS norm of Δp:

$$\varepsilon_{min} = \min \Delta p(\vec{r}) \tag{3}$$

$$\varepsilon_{max} = \max \Delta p(\vec{r}) \tag{4}$$

$$\varepsilon_{RMS} = \sqrt{\frac{1}{V}\int_V \Delta p(\vec{r}) dV}. \tag{5}$$

Table 8: Comparison of the power distribution obtained with PEBBED and Rattlesnake. The difference is quantified by the RMS norm, minimum, and maximum value of the relative difference of the power distributions in percent.

	p0			p1			p2			p3			p4			p5		
	RMS	Min	Max	RMS	Min	Max	RMS	Min	Max	RMS	Min	Max	RMS	Min	Max	RMS	Min	Max
r0	28.2	-13.5	84.8	22.0	-8.4	72.4	18.4	-5.8	64.8	18.5	-5.7	64.9	14.0	-4.2	58.0	11.6	-3.6	54.5
r1	27.5	-15.5	85.9	21.2	-6.9	74.6	17.2	-5.3	70.5	17.3	-5.0	70.5	12.6	-3.3	63.1	10.1	-2.7	59.8
r2	27.1	-17.0	86.6	20.6	-9.8	78.2	16.6	-4.5	72.6	16.5	-4.8	72.6	11.6	-3.1	66.8	9.1	-2.6	62.4
r3	26.7	-18.0	86.5	20.1	-11.4	79.5	15.9	-5.6	74.4	15.9	-5.3	74.3	10.9	-3.6	67.4	8.2	-3.1	63.6
r4	26.4	-19.3	86.4	19.6	-12.2	80.0	15.3	-6.2	74.9	15.3	-6.1	74.8	10.2	-4.3	68.1	7.6	-3.8	64.4

The results are presented in Table 8. We observe that ε_{RMS} and ε_{min} diminish as both meshes are refined, while ε_{max} remains large. The spatial distribution of the relative differences for PEBBED's p0 through p5 meshes is plotted in Fig. 9; MAMMOTH's mesh is fixed to r4. The maximum relative difference occurs at the top of the pebble bed in a region immediately adjacent to the top cavity. As the PEBBED mesh is refined, the size of the region decreases but the magnitude of the error remains almost constant. This leads to non-convergence of the two power distributions in the maximum norm, and slow convergence in the RMS norm.

These convergence properties are established for functions that converge pointwise except for a region of measure zero [46]. A region of measure zero is defined as a subset of the geometry whose volume limits to zero as the meshes are refined. The reason why MAMMOTH and PEBBED disagree at the top of the pebble bed is unknown. We conjecture that this is ultimately caused by the drop in density across the pebble bed/top cavity interface, because the power densities agree significantly at all other pebble bed/reflector interfaces. The proximate cause of the discrepancy, a deficiency or difference either in the code or the numerical method, is, however, unknown. Further investigation via mesh refinement is stymied by the lack of flexibility of the PEBBED code.

Another possible reason for the comparatively large error in the power density at the top of the core is insufficient refinement of the axial reflector region. The axial reflector region is refined to about $\Delta h_a 10$ cm in order to be able to focus on the core and control rod regions. The lack of mesh refinement may be insufficient and the lack of reduction of error with mesh refinement may ultimately be caused by the lack of mesh refinement in the top reflector.

The large value of Δp for the p0 and p1 meshes in Fig. 9 at the right boundary immediately below the top of the pebble bed is caused by insufficient refinement of the control rod, which is inserted to a depth of 170 cm below the top of the pebble bed. The finite difference method implemented in PEBBED requires exceedingly small mesh elements in the vicinity of the control rod to obtain reasonably accurate results. In particular, refinement steps p4 and p5 refine the control rod and adjacent fuel areas leading to significantly better agreement between PEBBED and MAMMOTH around the upper right corner of the pebble bed.

In conclusion, simultaneous mesh refinement of both MAMMOTH and PEBBED leads to better agreement of the computed power distributions. However, the two power distributions do not appear to converge pointwise, i.e. in the maximum norm, which may be attributed to different treatment of the low density cavity region or lack of mesh refinement

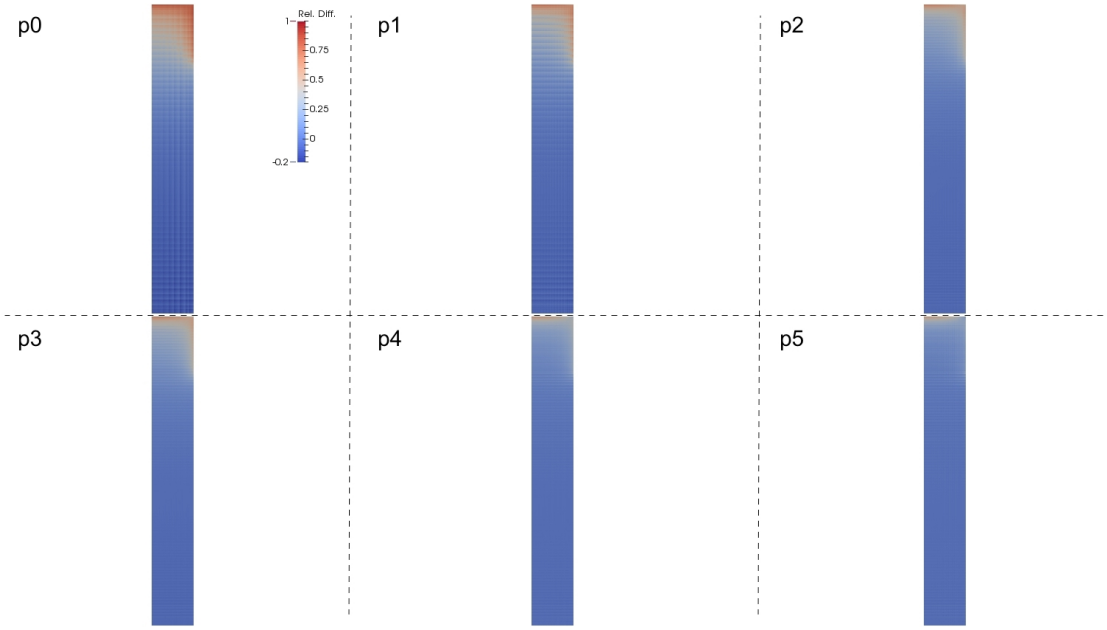

Figure 9: Relative difference of PEBBED and MAMMOTH power distributions computed using the MAMMOTH r4 mesh refinement level. Note: relative difference is not in percent.

in the top reflector of the PEBBED model. Further mesh refinement is impossible because of limitations in the PEBBED code.

4.1.2 Stand-Alone Thermal-Fluids

This section compares results of THERMIX-KONVEK with Pronghorn. The power density constituting the heating rate is taken from PEBBED and imported into Pronghorn as piecewise constant function. We adopt the strategy to import the power density from the most refined, available mesh. For this study, this is the p3 mesh described in Table 2. Meshes p4 and p5 were not available when this study was performed and adding them is not expected to change the conclusions of this section.

We compare the solid and fluid temperature computed by Pronghorn (PH) and THERMIX (TX). The difference of the solid and fluid temperatures is computed as $\Delta T = T_{\mathrm{PH}} - T_{\mathrm{TX}}$ for the p0 through p3 meshes using the r3 Pronghorn mesh as reference. The distribution of the temperature differences for the fluid and solid are plotted in Figs. 10 and 11, respectively.

The differences of THERMIX and Pronghorn computed solid and fluid temperatures are in excess of 50 K at the radial core/reflector boundary close to the bottom of the active core. For the most converged meshes, comparing r3 and p3, the minimum remaining difference is -72 and -80 K for the fluid and solid temperatures, respectively. The temperature fields are visually converged ruling out residual discretization error as cause for the disagreement. Throughout most of the reactor, the differences between Pronghorn and THERMIX are significantly smaller than the maximum values:

- Roughly 20 K for both solid and fluid temperatures along the core center line.
- The RMS norm of ΔT for the fluid and solid fields is 10 and 16 K, respectively.

We theorize that the difference between Pronghorn and THERMIX is caused by how the interface between pebble bed and reflector is treated. This conjecture is based on the location of the maximum of the difference in computed temperatures which is close to the core-reflector interface. The lineouts in Figs. 10 and 11 show significant qualitative differences between the THERMIX and Pronghorn solutions. The THERMIX temperature distributions almost have a horizontal tangent, while the Pronghorn solutions are much steeper.

Several potential causes for the discrepancy are assessed and found to not cause the difference in temperatures:

- To the best of the author's knowledge THERMIX does not account for conjugate heat transfer. For consistency, conjugate heat transfer is not included in the Pronghorn model.
- The vertical component of the fluid velocities are in relatively good agreement: at an elevation of 2.5 m and at a radial distance of 1.5 m Pronghorn computes 9.9 $\mathrm{m/s}$, while THERMIX computes 10.2 $\mathrm{m/s}$.
- The computed heat transfer coefficient α describing the exchange of heat between fluid and pebbles is in relatively good agreement: at an elevation of 2.5 m and at a radial distance of 1.5 m Pronghorn computes 1.72×10^5 $\mathrm{W/m^2K}$, while THERMIX computes 1.68×10^5 $\mathrm{W/m^2K}$.

Further investigation finds that THERMIX solves fluid flow equations and computes a convective heat source in the first layer of reflector elements right outside of the core. Refinement steps p2 and p3 reduce the size of the elements right outside the pebble bed in order

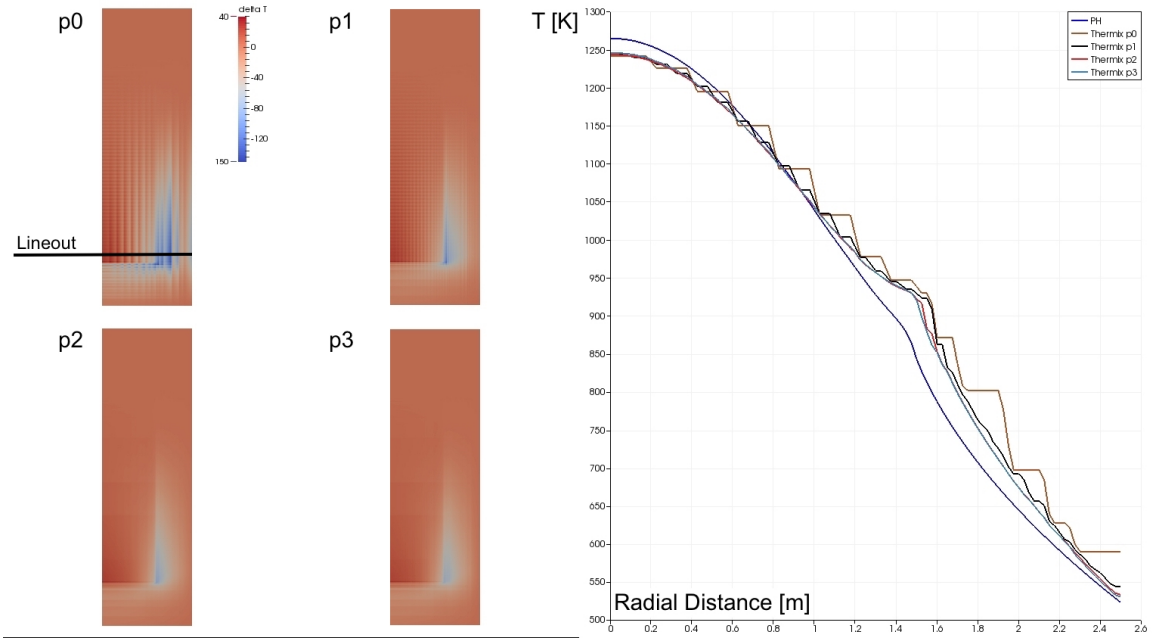

Figure 10: Difference of the solid temperatures computed by Pronghorn using the r3 mesh and THERMIX computed with meshes p0 through p3. A line-out is presented at elevation $z = 2.4$ m.

to limit the influence of this possible inconsistency. Reduction of the difference is observed for the p2 refinement step, but no additional improvement occurs for the p3 refinement step. It is unclear whether the extension of the heat source into the reflector is intentional, e.g. for taking into account conjugate heat transfer. It is also unclear whether it is the cause of the difference of the Pronghorn and THERMIX results. The resolution of this question is impeded by the lack of documentation of the THERMIX-KONVEK solver.

We believe that further investigation into the described discrepancy is not valueable due to the lack of documentation and maintenance of the THERMIX code.

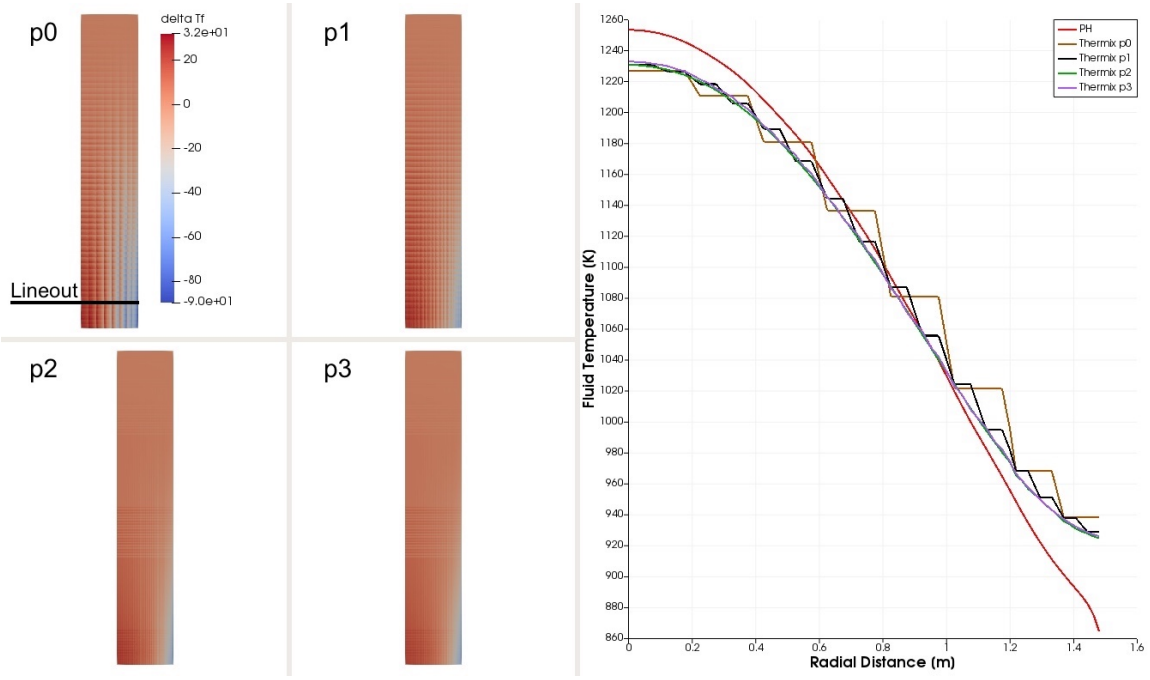

Figure 11: Difference of the fluid temperatures computed by Pronghorn using the r3 mesh and THERMIX computed with meshes p0 through p3. A line-out is presented at elevation $z = 2.4$ m.

4.1.3 Coupled Steady-State

The comparison of coupled N/TH calculations between MAMMOTH/Pronghorn and PEB BED-THERMIX-COMBINE could not be performed because of deficiencies in the peripheral capabilities in PEBBED-THERMIX-COMBINE. A fair and meaningful comparison can only be conducted if identical cross sections are used in both code systems. However, obtaining this cross section set from PEBBED is impeded by the discovery of multiple, successive coding errors. These errors are:

- PEBBED computes differing answers when provided with the same cross sections via cross section file and via standard input file. MAMMOTH agrees with the latter result but further comparison is delayed until this coding error is fixed.

- After the first coding error is fixed, it is discovered that cross section printouts after COMBINE updates, i.e. after taking into account thermal feedback, are incorrect. In

particular, all printed cross sections are zero.

Coupled comparisons between MAMMOTH/Pronghorn and PEBBED-THERMIX-COMBINE are hence not pursued because the process for using this code system as a cross section preparation tool is not mature enough. All attempts to prepare consistent cross sections failed despite significant time invested in correcting code errors in PEBBED. The PEBBED-THERMIX-COMBINE is a research code and does not possess the needed quality assurance pedigree to perform this type of calculations. Consequently, a decision was made to proceed with Serpent cross sections. Furthermore, there are also open questions about the level of documentation and capabilities of THERMIX-KONVEK. It is preferred to benchmark Pronghorn via experiments or reference CFD solutions.

4.2 Advanced Modeling

In this section we demonstrate the ability of MAMMOTH/Pronghorn for detailed, three-dimensional modeling of HTR-PM. The legacy tools are not capable of providing three-dimensional models. Moreover, comparison of *r-z* and detailed three-dimensional models is pointless, because substantial difference in the behavior of control rods in these models. In *r-z* geometry, control rods act as curtains that all neutrons streaming outwards at a certain elevation have to pass, while the same is not true in three-dimensional geometry. The advanced modeling uses the tool-chain comprised of LAMMPS, Serpent, and MAMMOTH/Pronghorn.

4.2.1 Discrete Element Simulations for HTR-PM

Discrete element (DEM) simulations provide the pebble positions for Serpent cross section calculations. Within this work, LAMMPS replaces the previously used PEBBLES code because the size of HTR-PM problem, namely 420,000 pebbles, leads to prohibitive run times of the PEBBLES code. Modeling efforts on the HTR-10 benchmark problem are possible with PEBBLES [18] because the number of pebbles is limited to roughly 25,000. A typical DEM simulation as required for this work is composed of two stages: first, the pebbles are introduced into the vat either all at once or in batches, and second, the pebbles are recirculated until the bed settles into a dynamic equilibrium state. The wall-clock time required to reach the dynamic equilibrium of the pebble bed is listed in Table 9. It should

be pointed out that all listed execution times are obtained with ad-hoc, and possibly sub-optimal, parameters like time step size and pebble removal frequency at the exit chute. The important observation is that execution times for PEBBLES are in excess of 4 weeks, while a LAMMPS simulation can be completed within a single day. The turn-around time of 4 weeks for completion of the DEM calculations is deemed unacceptable for the purpose of a PBR analysis sequence. LAMMPS' advantage is mainly due to the massively parallel architecture that is in sharp contrast to the multi-threaded PEBBLES code.

Table 9: Execution times for LAMMPS and PEBBLES for the HTR-10 and HTR-PM problems.

Parameter	HTR-10	HTR-PM
Number of pebbles	17,000	420,000
PEBBLES	$\approx$ 1 day	$>$ 4 weeks (32 threads)*
LAMMPS	$\approx$ 2.1 hours (24 CPUs)	$\approx$ 17.5 hours (432 CPUs)

* Bed is not sufficiently recirculated within the maximum wall clock time.

The LAMMPS DEM model is comprised of a cylindrical vessel that is 14 meters tall, and 3 meter in diameter. The vessel is taller than the actual HTR-PM vessel to prevent pebbles deflecting off each other and interacting with the top boundary which is a rare but possible numerical artifact caused by the extremely stiff interaction potentials. Below the vessel is a lower conus and exit chute whose dimensions follow Table 4. Top and bottom boundaries are either solid walls or periodic boundary conditions depending on the phase of the LAMMPS simulation.

Pebbles interact with other pebbles and solid walls via single-point contact forces. The contact forces are computed from the *pair_style* potentials available in LAMMPS' granular flow model. LAMMPS provides multiple models for contact forces that can be divided into the two main categories of Hookean and Hertzian potentials. The simplest Hookean potential: *pair_style gran/hooke* is selected in this work. We follow the recommendation of Ref. [16] for parameterizing the Hookean contact model; these parameters are provided in Table 10.

The LAMMPS simulations in this work are initiated by introducing all pebbles into the reactor simultaneously as a face centered cubic (fcc) array with a lattice constant of 9 cm. To ensure that roughly 420,000 pebbles are introduces the fcc lattice is confined within a cylindrical insertion region of proper radius and height. The lower end of the insertion

Table 10: LAMMPS parameterization for HTR-PM.

Parameter	Symbol	Value	Unit
Characteristic time constant	τ	0.0782	s
Elastic normal repulsion	k_n	5.9×10^7	N/m
Elastic tangential repulsion	k_t	$2/7 k_n$	N/m
Normal viscoelastic constant	γ_n	$\frac{158.1}{\tau}$	s^{-1}
Tangential viscoelastic constant	γ_n	$\frac{79.06}{\tau}$	s^{-1}
Friction coefficient	μ	0.35	
Time step relaxation phase	Δt_x	1.96×10^{-6}	s
Time step recirculation phase	Δt_r	3.91×10^{-5}	s

region is one pebble diameter above the bottom of the cylindrical part of the HTR-PM vessel. Both top and bottom of the simulation domain are closed. Before the start of the simulation, the each pebble's position is randomly perturbed up to a distance of ± 3 cm is each direction. When the simulation starts, gravity accelerates the pebbles downwards until they deflect of the vessel and start to fill up the chute region. The initial part of the simulation continues until all pebbles have settled, i.e. the total kinetic energy of the system is low which is achieved after roughly 2.5 seconds of simulation time. During the second phase of the LAMMPS simulation the pebbles are recirculated. This is achieved by opening up the bottom and top boundaries of the geometry and imposing periodic boundary conditions. Pebbles leaving through the exit chute outlet reappear at the top of the vessel at $z = 14$ m. The recirculation rate of pebbles is controlled by a viscous force

$$\vec{F} = \gamma \vec{v}, \tag{6}$$

where $\vec{F}$ is the force and $\vec{v}$ is the pebble velocity that is applied for pebbles within 30 cm of the bottom boundary. The constant γ is chosen to provide sufficient separation between pebbles leaving the vessel's bottom and being re-introduced at the top such that only a small fraction of the pebbles are ever in flight from the top of the vessel towards the top of the pebble bed.

Simulation time and real time can be correlated to each other by the accumulated number of pebbles that have been recirculated, i.e. pebbles leaving through the bottom boundary that are reintroduced through the top boundary. In the current simulation roughly 75 pebbles are recirculated per second of simulation time. In typical reactor operations, the fuel handling system removes roughly $5,000$ pebble per day, so that each second of simulation time corresponds to roughly 1300 seconds of reactor operation.

Of particular interest to the DEM simulation of PBRs is the packing fraction η defined as:

$$\eta = \frac{V_s}{V_s + V_g}, \tag{7}$$

where V_s is the volume occupied by solid and V_g is the fraction occupied by Helium gas. We compute the integral packing fraction of the bed from the height of the cylindrical portion, the number of pebbles comprised within this portion and the original volume. In addition, we compute the packing fraction for cylindrical subsections with a thickness of 1 meter of this bed by computing the volume of the subsection and the number of pebbles contained within the subsection. Pebbles are considered within a subsection if the centroid of the pebble is within the subsection. This analysis is performed for the last snapshot of pebble positions. The results are accumulated in Table 11.

The packing fraction computed by LAMMPS is higher than expected but within the band of experimentally and computationally obtained results. The underlying reason for the spread of packing fractions is not fully understood by the authors and requires further investigation. We find 0.6353 as overall packing fraction and between 0.637 at the bottom of the bed and 0.6329 at the top of the bed. Commonly, the packing fraction is assumed to be around 0.61, e.g. for the annular PBMR design [47] and for HTR-10 [41]; it is uncertain how this number is obtained. Compaction during earthquakes is investigated in the Samson experiment and is limited to 0.616 [48]; however, a much more conservative value of 0.64 is adopted for earthquake related safety analysis [47]. Experiments to determine the packing fraction of randomly packed beds of spheres in cylinders are performed by [49] and [50] who find a limit of 0.61 and 0.6336 for large cylinders, respectively. In both references, the beds are created as randomly loose packed bed and then shaken until the bed height cannot be further reduced. A survey of computational and experimental packing fractions in Ref. [51] finds a significant spread of packing fractions ranging from 0.55 to 0.65. The same reference finds by computational simulations with the LAMMPS derived LIGGGHTS code [52] that the packing fractions depend on how the bed is prepared and the material properties of the spheres (density and elastic modulus): packing fractions ranging from 0.58 to 0.636 are computed.

The local packing fraction is computed using the Voronoi analysis included in the Ovito visualization tool [53]. This is accomplished by taking the ratio of each pebble volume and the atomic volume defined as the volume allotted to each pebble. Results are depicted in Fig. 12 for several snapshots during the preparation of the bed. After introduction of the pebbles, the packing fraction is very large because the pebbles are compacted into the original fcc lattice. During recirculation, the high density regions are flushed out and after sufficient time has passed, the bed settles into its dynamic steady state. The packing fraction

Table 11: Integral packing fraction computed by LAMMPS.

Z_{min}	Z_{min}	η	Number of pebbles
0	10.124	0.6353	401,378
0	1	0.6365	39,780
1	27	0.637	39,809
2	3	0.6356	39,726
3	4	0.6356	39,722
4	5	0.6354	39,711
5	6	0.6361	39,754
6	7	0.6358	39,736
7	8	0.635	39,690
8	9	0.6349	39,683
9	10	0.6329	39,559

slightly increases from top to bottom because pebbles are compressed under the weight of the pebbles above them. LAMMPS models the deformation of pebbles as slight overlap. In contrast to [51], the overlap is not considered for computing the packing fraction, namely the volume of the pebbles is assumed to be constant. We note that Pronghorn is capable of taking into account spatial variations in the porosity. Future work will use this advanced feature to create a more accurate representation of the pebble bed in Pronghorn.

We suggest a thorough investigation of the current method for predicting pebble centroid positions in PBRs. The primary goal of this investigation is to qualify the current computational approach based on LAMMPS. The secondary goal is to understand the significant spread of published results by understanding differences in the deployed experiments and models and identify the key parameters determining the characteristics of pebble beds.

4.2.2 Serpent high-resolution

The physical verification of the neutronics model involves the calculation of key reactor physics parameters. This task is impeded by the lack of published results for systems with this exact fuel enrichment and the given ratio of fuel to dummy pebbles. Therefore, a more qualitative approach is warranted. Table 12 provides various eigenvalues at different control rod positions as well as control rod worths. The control rod worth at the fully inserted

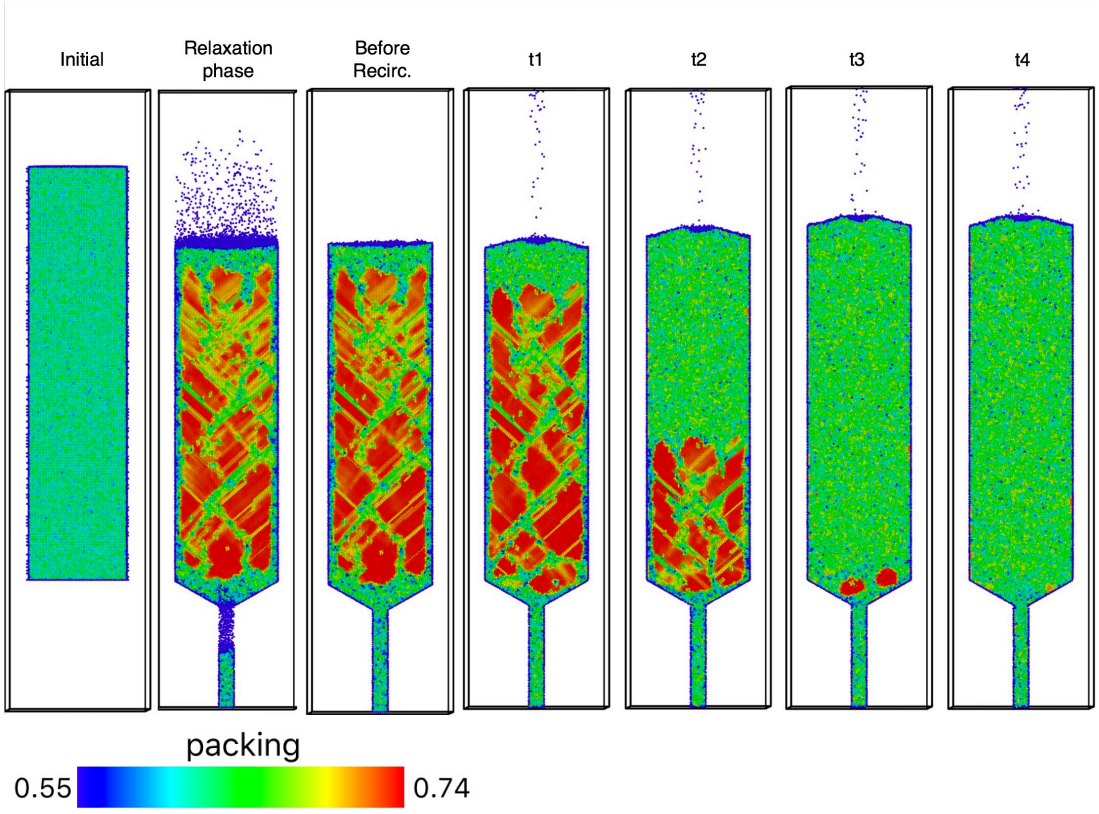

Figure 12: Packing fraction computed by LAMMPS for HTR-PM during the simulation: pebbles are introduced as randomly perturbed fcc array and then dropped (Initial), then allowed to relax until most kinetic energy is dissipated (relaxation and before recirculation). Finally, pebbles are recirculated until the bed achieves its dynamic equilibrium (t_1 through t_4).

position is calculated at 3.37% $\Delta k/k$. The HTR-Module design employed 6 control rods with an insertion depth that did not extend the full height of the pebble-bed. The worth of those rods, 1.2% [54], compares well with the worth calculated here for 8 rods at a similar depth (1.37%).

The calculated excess reactivity for the core at room temperature with all rods withdrawn in Table 12 appears high, $\sim$15.4% $\Delta k/k$. The reactivity requirement for a cold shutdown on the secondary shutdown system (SSD) would be $\sim$12% with ARI, which is in the vicinity of the 10.8% worth of the SSD in HTR-Module.

Table 12: Control rod worth at 300 K

control rod position [cm withdrawn]	k_{eff}	Uncertainty $[pcm]$	worth [%]
1,130.0 (ARO)	1.15407	5.1	
0.0 (ARI)	1.11082	13	3.37
680.0	1.13615	6.3	1.37

For operation at temperature, Table 13 presents eigenvalues at the various state points introduced in Table 6. The average core temperature at power is expected to be near 800 K, thus one can predict a k_{eff} value of the coupled N/TH model of roughly 1.05. In addition, one must consider the effect of initial fission product buildup, which, for this core, is calculated with Serpent to be $\sim$2% $\Delta k/k$. This leaves roughly 3% of unbalanced reactivity at power, which implies that the core must operate with deeply inserted rods or higher temperatures to remain critical. A related point to consider is that the V.S.O.P. calculations, on which this core configuration are based [44], might contain significant uncertainty. In addition, there is also some uncertainty due to the higher than usual packing fraction produced by the pebble mechanics simulations compared to the standard 0.61 assumption, but the reactivity difference is expected to be small ($\sim$0.5%) based on pebble-bed compaction results from [55].

The temperature coefficient of reactivity presented in Table 14 is the total temperature feedback mechanisms for an HTR (i.e. fuel, moderator, reflector). It is noted that the reflector temperatures used in this calculation are not isothermal. The calculated values are higher than the value of 11% calculated for the HTR-10 [18], but they are consistent with the order of magnitude computed for the HTR-Module [56]. Furthermore, one must consider the fact that the low enrichment of the fuel and the increase in the amount of graphite in the core will lead to significantly higher temperature coefficients of reactivity.

In conclusion, all of these reactor physics parameter values are credible and consistent with the similar designs thus the physical validity of the model is confirmed.

Table 13: Reference k_{eff} at each state-point

Tsolid $[K]$	k_{eff}	Uncertainty $[pcm]$
500.0	1.11318	1.6
700.0	1.07344	1.7
900.0	1.04054	1.7
1100.0	1.01159	1.8
1300.0	0.98622	1.8

Table 14: Reference temperature coefficient of reactivity

Temperature range $[K]$	Temperature coefficient $[pcm/K]$
500 - 700	-16.63
700 - 900	-14.73
900 - 1100	-13.75
1100 - 1300	-12.72

4.2.3 Three-dimensional homogenized MAMMOTH model

Table 15 presents the eigenvalues computed with MAMMOTH and differences with respect to the reference Serpent calculation in pcm. Two solutions are provided 1) diffusion (Diff) and 2) transport-corrected diffusion with tensor diffusion coefficients and SPH (Diff-TDC-SPH). The diffusion solution mesh is spatially converged by forcing two uniform refinement levels. This effectively divides each initial element into 64 elements and renders a system with 14,109,060 DoFs. The transport-corrected diffusion solutions retains the base mesh and produces a system with 226,176 DoFs.

The metrics for the fission and absorption distributions within the SPH corrected regions are included in Tables 16 and 17. Without the SPH treatment the diffusion solver displays a clear bias in k_{eff}. The bias increases with temperature to a maximum value of 2600 pcm. Furthermore, the RMS error in the fission distribution is 6% with a maximum error of 41%. The absorption rates are substantially worse with an RMS larger than 14% and maximum over 170%. Conversely to these results are those obtained with transport corrected diffusion, which recover the reference Serpent solution in the SPH regions, even with 4 energy

groups. The RMS and maximum errors are very small ($< 0.005\%$).

Table 15: Calculated k_{eff}. Differences versus reference Monte Carlo solution in pcm in parenthesis

Tsolid $[K]$	Diff	TDC-SPH-Diff
500.0	1.13384 (1856.1)	1.11318 (0.0)
700.0	1.09517 (2024.3)	1.07344 (0.0)
900.0	1.06472 (2324.2)	1.04054 (0.0)
1100.0	1.03653 (2464.9)	1.01159 (0.0)
1300.0	1.01179 (2593.3)	0.98622 (0.0)

Table 16: Calculated % rel. diff. in fission ($\nu\Sigma_f$) reaction rates

Tsolid	Diff		TDC-SPH-Diff	
$[K]$	RMS	max	RMS	max
500	5.86E+00	4.10E+01	2.13E-04	4.78E-04
700	6.14E+00	4.14E+01	1.95E-04	3.88E-04
900	6.17E+00	4.12E+01	1.55E-03	3.40E-03
1100	6.00E+00	4.06E+01	1.55E-03	2.94E-03
1300	6.04E+00	4.03E+01	2.84E-04	4.58E-04

Table 17: Calculated % rel. diff. in absorption reaction rates

Tsolid [K]	Diff RMS	Diff max	TDC-SPH-Diff RMS	TDC-SPH-Diff max
500	1.42E+01	1.73E+02	2.35E-04	4.84E-04
700	1.44E+01	1.74E+02	2.17E-04	4.28E-04
900	1.45E+01	1.73E+02	1.75E-03	3.62E-03
1100	1.44E+01	1.71E+02	1.69E-03	3.15E-03
1300	1.44E+01	1.72E+02	2.91E-04	4.60E-04

The calculated total temperature coefficient of reactivity based on the various state-points is plotted in Figure 13. The k_{eff} bias in the eigenvalue calculations with the diffusion solver translate directly to a feedback bias and will produce a lower temperature feedback in coupled solutions. The Serpent and transport-corrected diffusion solutions are indistinguishable.

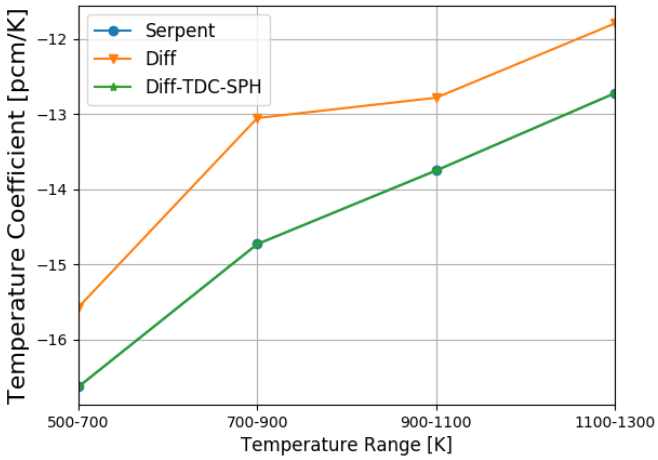

Figure 13: Temperature coefficient of reactivity

4.2.4 Three-dimensional Coupled MAMMOTH-Pronghorn Calculations

In this section, we present steady-state, multiphysics results for the utilized three-dimensional HTR-PM model at an operating power of 250 MW(th). We compare the power density of

coupled simulations with SPH correction, without SPH correction, and without feedback, i.e. cross sections being evaluated at 523 K. Other quantities of interest such as solid temperature, fluid temperature, pressure, and velocities are discussed. We exercise the conjugate heat transfer capability and compare the obtained results to the base case that does not use the conjugate heat transfer capability.

The emphasis of this section is presentation of the existing capabilities, description of the approach to obtain the coupled solution, qualitative assessment of the solution, and identification of missing capabilities.

The multiphysics coupling between neutronics and fluid fields occurs through two variables: the power density computed from the fission distribution acts as heat source in the TH equations, and the solid temperature computed by TH modifies the cross sections used in the neutronics calculation. The power density is an *auxiliary* variable that for convenience we think of as being part of the neutronics set of equations, while the solid temperature is a *nonlinear* variable of the TH system.

Table 18: Eigenvalues for the coupled, three-dimensional HTR-PM MAMMOTH-Pronghorn model.

Case	Eigenvalue
Temperature feedback, SPH correction	1.0506
Temperature feedback, no SPH correction	1.0709
No temperature feedback	1.109

MAMMOTH-Pronghorn offers two approaches for solving the coupled system of equations. In the *fully coupled* approach all equations can be solved in a single nonlinear system of equations, and in the *tightly coupled* approach the neutronics and thermal hydraulics equations are solved separately after one another exchanging updated power distributions and solid temperature fields. The latter approach uses Moose's multiapp system [26] that is designed with transient problems in mind:

1. Neutronics is the master-app and is solved first.
2. Power distribution is updated in the TH system.
3. TH problem is solved.
4. The solid temperature is updated in the neutronics system.

5. A consistency check is performed and if satisfied, the solutions moves on to the next timestep. If the consistency check is not satisfies, repeat this process starting at 1.

This iteration process is referred to as Picard iteration. For the solution of the steady problem, a similar iterative process is used. The sub-app:Pronghorn is solved to full convergence at the beginning of each nonlinear iteration of the master-app:MAMMOTH, but no explicit consistency check is performed. Reduction of the nonlinear residual of the master-app signals that a neutronics solution that is consistent with the temperature distribution is found.

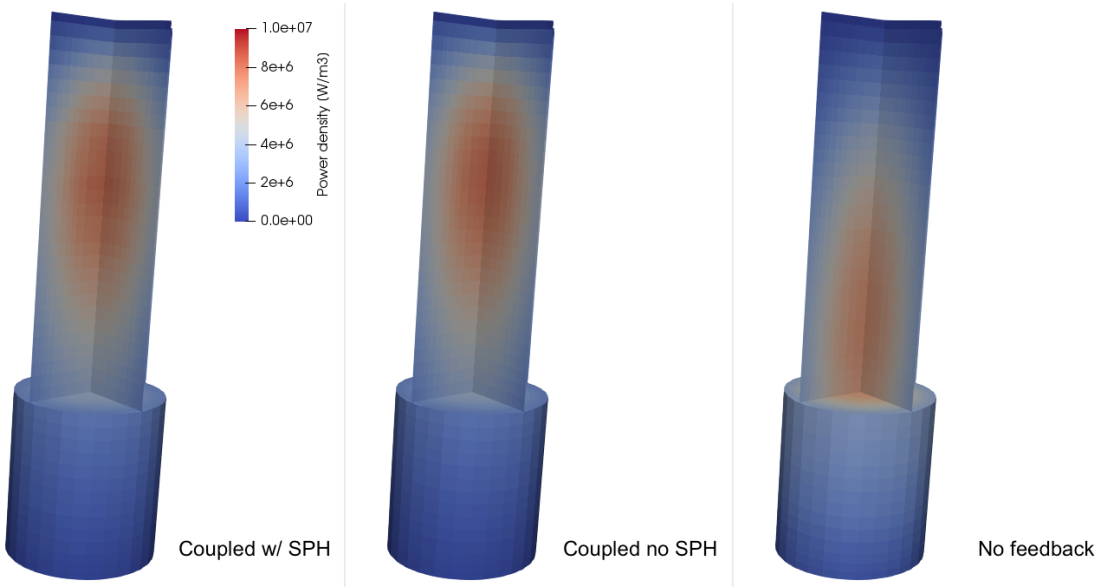

Figure 14: Power densities computed for the three-dimensional HTR-PM model using MAMMOTH-Pronghorn. Coupled with SPH uses a coupled MAMMOTH-Pronghorn calculation with applying SPH, Coupled no SPH uses a coupled MAMMOTH-Pronghonr calculation without applying SPH, and No feedback evaluates all cross sections at 523 K corresponding to cold conditions.

Convergence of the coupled, three-dimensional steady-state problem proves to be challenging. Typically, TH problems are solved for transients where the initial condition is known. Nonlinear convergence problems can be mitigated by reducing the time steps and thus change from the last known solution. In this case, we solve a neutronics eigenvalue problem coupled with a steady-state TH problem. Convergence is precluded if the TH initial guess is too far from the converged solution.

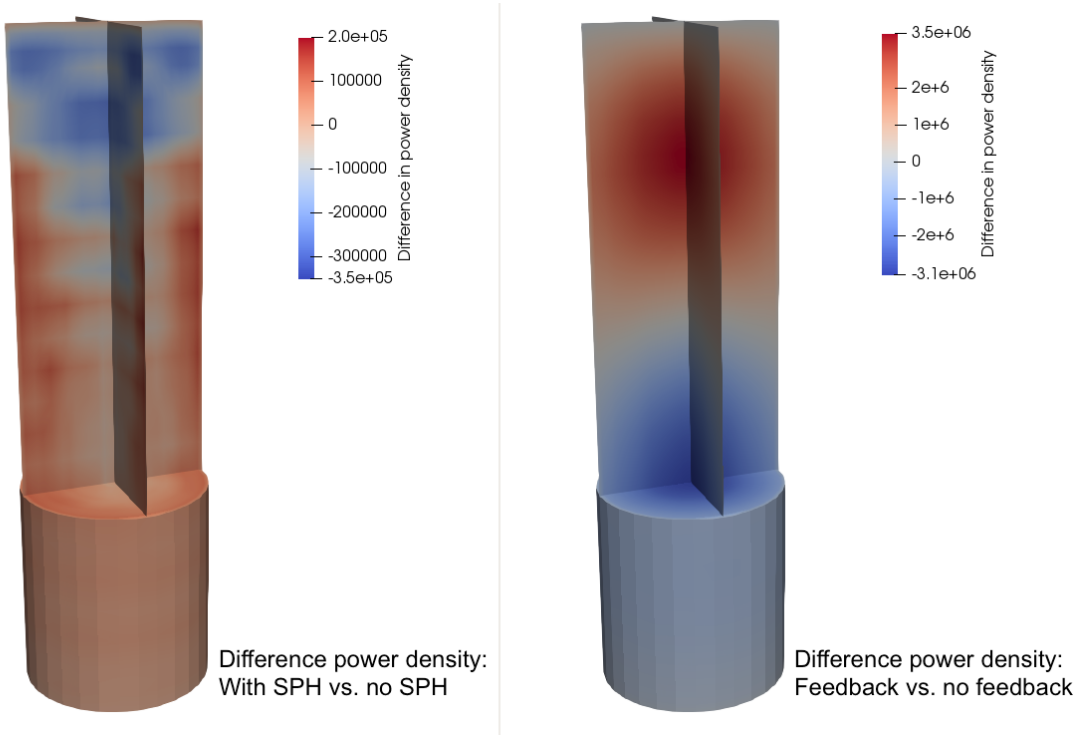

Figure 15: Difference in power densities comparing SPH vs. no SPH on the left and feedback and no feedback on the right. Significant differences in both cases are observed but larger differences result from the inclusion of feedback. The power peak clearly migrates up due to the comparatively colder fuel in the upper part of the pebble bed.

We found that it is necessary to generate an initial guess via a de-coupled Pronghorn pseudo transient calculation. A pseudo transient is a transient calculation that is solved to very large simulation times at which the system has reached its steady state. This steady state is identical to the solution of the original steady-state problem that we are interested in. Using a fixed uniform heat source distribution allows for solving Pronghorn independently from MAMMOTH and obtaining a sufficiently accurate initial guess for allowing the coupled steady-state problem to converge.

Steady-state calculations are performed using both fully and tightly coupled algorithms. The converged results are identical to within iterative convergence criteria. Even with the improved initial guess, we find the following settings to be absolutely essential to achieve convergence:

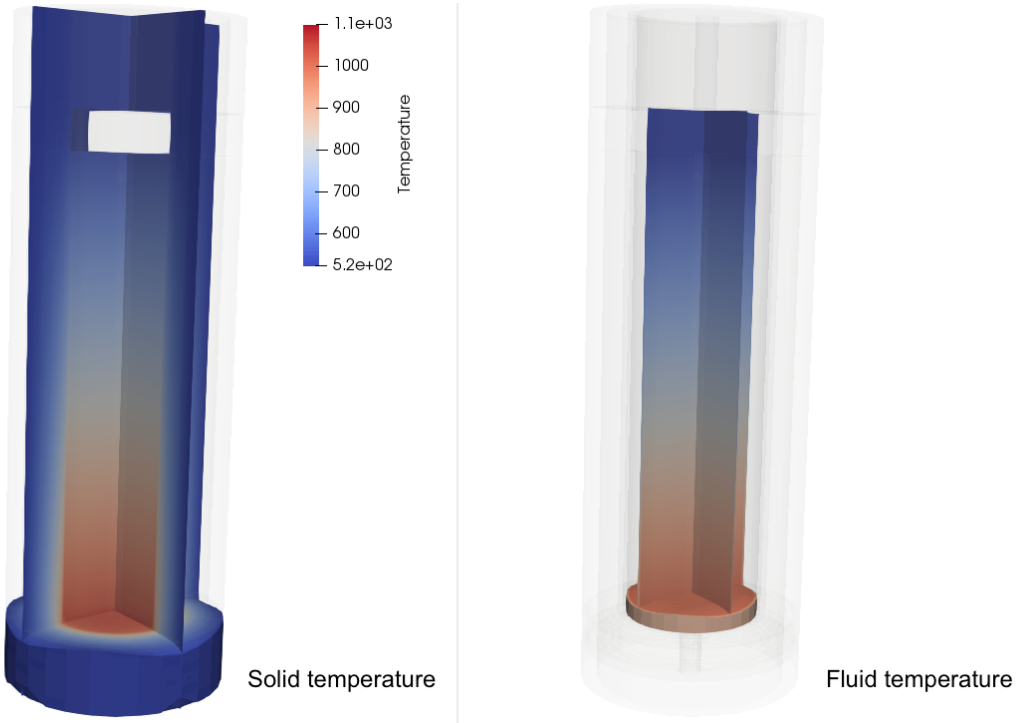

Figure 16: Solid and fluid temperature distribution obtained with the coupled MAMMOTH-Pronghorn model with application of SPH. For orientation, the model outline is added as shading.

- Sufficient number of initial free power iterations. While the exact minimum number is not determined, we use 6 and 10 for fully and tightly coupled simulations.
- Inclusion of sufficient off-diagonal terms of the TH equations in the Jacobian. We use all off-diagonal terms but a more judicious choice may conserve favorable convergence properties and reduce memory consumption.
- Proper inversion of the Jacobian: we find that only *super lu* properly inverts the Jacobian including both neutronics and TH terms. Any other iterative method fails to provide sufficient preconditioning. However, the matrix factorization of *super lu* is very expensive to compute for three-dimensional problems. Nevertheless, linear convergence is still relatively slow as outlined in the next bullet.
- Sufficient linear convergence for each nonlinear step: we allow 75 linear iterations per nonlinear and use a (relative) linear tolerance of 1×10^{-4}

- *l2* line search must be used.

A judicious choice of solver parameters is required to prevent the solution to obtain impermissible values of the variables leading to failure when evaluating correlation equations, e.g. evaluating a square root with a negative temperature. These issues result in a comparatively slow and unstable convergence behavior. We recommend to invest significant resources to develop robust and fast iterative methods for coupled MAMMOTH-Pronghorn models.

Both fully and tightly iterative schemes converge. The fully coupled scheme converges using 6 initial power iterations and an additional 13 nonlinear iterations. The tightly coupled scheme requires 10 initial power iterations and and additional 39 nonlinear iterations. The larger number of nonlinear iterations for the tight coupling is caused by the slow convergence of the initial nonlinear residual of the Pronghorn sub-app. In this study we opted to ensure proper convergence of the sub-app measured by the first nonlinear iteration of each sub-app call to Pronghorn because it constitutes a consistency check of the freshly computed power distribution. As this check is not naturally performed in Moose, the convergence criterion of the master app is tightened significantly and is possibly set to an unnecessarily small value. Additional studies should be performed to assess feasibility and efficiency of tightly coupled simulations.

We present power densities, differences of power densities computed with SPH/non-SPH and feedback/no-feedback, solid and fluid temperatures, and pressure and vertical speed in Figs. 14 through 17. Eigenvalues for the coupled SPH corrected, coupled uncorrected, and no temperature feedback cases are listed in Table 18. In the absence of a reference solution, we assess the result only qualitatively and find that it is physically reasonable. The reduction of the eigenvalue due to temperature feedback is 5000 pcm (cases 1 and 3 in Table 18). This value is consistent with the temperature feedback coefficient of reactivity and an isothermal temperature rise of roughly 300 K (523 K to 823 K). This result is in agreement with the estimate based on isothermal temperature coefficients of reactivity in section 4.2.2.

The computed power densities for three cases: coupled MAMMOTH-Pronghorn with SPH, coupled MAMMOTH-Pronghorn without SPH, and MAMMOTH with solid temperature fixed at 523 K are shown in Fig. 14. In addition, the difference of power densities between cases 1 and 2 and cases 1 and 3 are plotted in Fig. 15. The distribution of solid temperatures causes a shift of the power density up to the colder regions of the core. The power density near the top of the core is up to $3.5 \times 10^6 \frac{\mathrm{MW}}{\mathrm{m}^3}$ larger than in the isothermal case, while the

power density near the bottom is 3.1×10^6 lower than in the isothermal case.

Using SPH is essential for obtaining an accurate power distribution. Even though the differences between power distributions of cases 1 and 2 are much smaller than the differences between cases 1 and 3, the relative differences still amount to 10s of percent of the nominal power density. The presented results exemplifies the feasibility of using SPH corrections in multiphysics MAMMOTH-Pronghorn simulations.

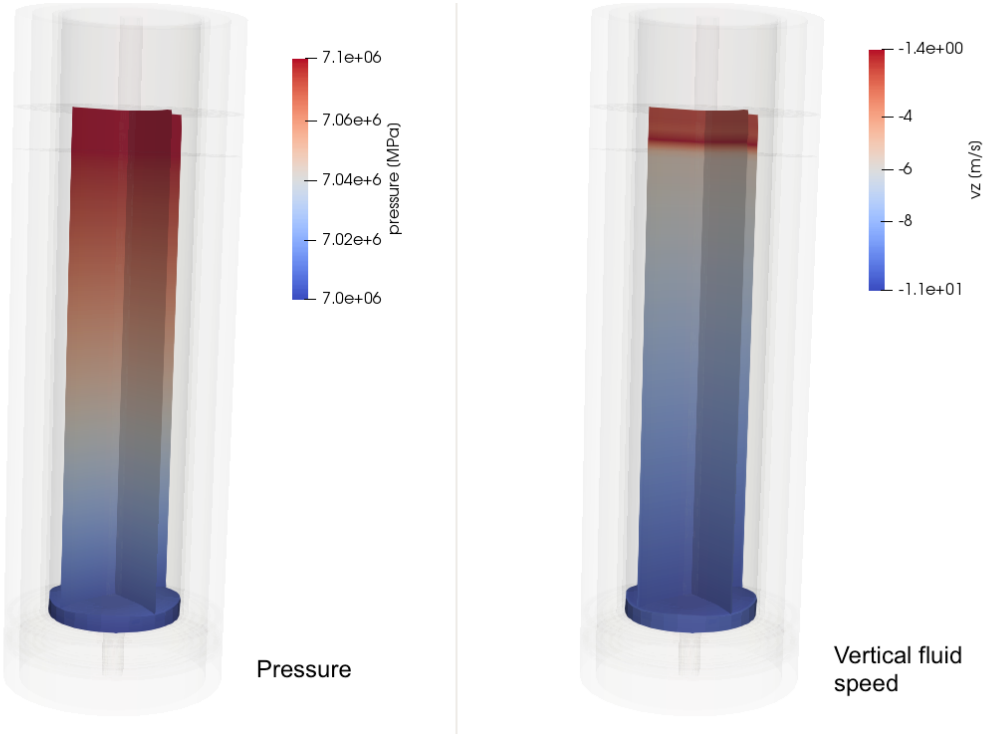

Figure 17: Pressure and vertical fluid speed v_z in the pebble bed and upper cavity obtained with the coupled MAMMOTH-Pronghorn model with application of SPH. For orientation, the model outline is added as shading.

Solid and fluid temperatures computed with the SPH corrected coupled model are presented in Fig. 16. The solid temperature at the outer boundary is 523 K as dictated by the Dirichlet boundary conditions and the highest temperatures, $\approx$ 1200 K, are observed at the center of the pebble bed right at the outlet. At the top of the pebble bed, the solid temperature is close to the inlet fluid temperature of 523 K. In all but the top reflector, the solid temperature steeply drops from the core temperature to the prescribed temperature on the boundary. The top reflector is separated from the core by the cavity where no solid temperature is

computed. In this work, radiative heat transfer is not taken into account through the cavity, but even if it were, the effect would be negligible because the fluid inlet temperature and the fixed boundary temperature are identical. This is not necessarily true in reality where the coolant is heated in the riser and boundary conditions at the fringes of the reflector have to model heat transport to the vessel.

The fluid temperature closely tracks the solid temperature in the active core region indicating a relatively constant ratio of per pebble heating generation rate and convective heat transfer coefficient. The temperature distribution of the fluid temperature over the outlet sideset satisfies conservation of energy.

Pressure and vertical coolant speed are depicted in Fig. 17. The pressure is fixed at 7 MPa at the outlet and the pressure drop over the pebble bed is 0.1 MPa. The fluid speed is negative because the flow direction is along the negative z-axis. Vertical fluid speed is lowest (in absolute value) in the cavity due to the higher porosity and increases in the pebble bed. Within the pebble bed, radial variations in fluid speed are small, while the speed increases axially due to a decrease of the coolant's density.

The impact of conjugate heat transfer on results and convergence behavior is small. The maximum relative differences of the computed variables between the models with and without conjugate heat transfer are listed in Table 19 and found to be less than one percent. While conjugate heat transfer is available in Pronghorn its impact on the solution is smaller than the uncertainty of the utilized correlations. The heat transfer coefficient from the fluid to the wall is computed using Wakao's correlations [23].

Table 19: Maximum relative differences of computed variables for models with and without conjugate heat transfer (CHT).

Variable	Unit	Value w/o CHT	Values w/ CHT	Relative difference [%]
Fluid temperature	K	728.6	730	0.19
Solid temperature	K	605.7	603.7	0.33
Vertical speed	m/s	-8.44	-8.45	0.09
Power density	W/m^3	4.06×10^6	4.07×10^6	0.04

In summary, the current capabilities in MAMMOTH-Pronghorn are promising but additional work is required to enhance efficiency and robustness. In particular, efficient preconditioning and careful parameter checking during the evaluation of correlations is recommended. Results for the three-dimensional HTR-PM model appear to be physical but a

quantitative comparison to a credible benchmark calculation for a more physically accurate PBR model is recommended. Conjugate heat transfer can be included in the model but it is shown to have relatively small impact on the obtained results.

5 Conclusions and Future Work

This report describes the assessment of multiphysics, steady-state PBR simulation capabilities of the MAMMOTH-Pronghorn codes. We define stylized *r-z* and three-dimensional HTR-PM problems. For the former, a comparison to the PEBBED-THERMIX-COMBINE code system is performed, while only MAMMOTH-Pronghorn results for the three-di mensional model are obtained.

A comparison of the different modules, neutronics and TH, with PEBBED-THERMIX-COMBINE is performed. We find reasonable agreement between MAMMOTH and PEB BED for stand-alone neutronics calculations. Eigenvalues agree to within 21 pcm, while the power density agrees well almost everywhere except at the cavity-pebble bed interface. The reason for the disagreement is unknown, but it may be caused by different treatment of the low density cavity region in PEBBED's diffusion solver or insufficient mesh refinement of PEBBED in the upper reflector region. PEBBED limits the number of mesh points per direction to 108 and 256 for the r and z-axes, respectively.

Stand-alone TH comparison of THERMIX and Pronghorn shows reasonable agreement of solid and fluid temperatures almost everywhere except at the pebble-bed/radial reflector interface. Difference of the solid temperature can be as high as 90 K in this region; moreover both the shape of the temperature curves differ qualitatively between THERMIX and Pronghorn: the former almost has a horizontal tangent, while Pronghorn computes a much steeper curve. Efforts into identifying the root cause of these differences find that THERMIX computes convective heat transfer in the first reflector mesh element outside of the pebble bed. Lack of documentation impedes any effort to determine if this is intentional to mimic conjugate heat transfer, a user error, or an error in the code.

Comparison of coupled calculations between MAMMOTH-Pronghorn and PEBBED-THER MIX-COMBINE was not completed because of shortcomings of PEBBED-THERMIX-COMBINE in the ability to create and print the necessary cross sections for a meaningful comparison.

A three-dimensional HTR-PM model is created and Serpent is used to create cross sections at a variety of core conditions. In this work, solid temperature is identified as the most important state variable to functionalize cross sections. Cross sections are created at isothermal core conditions. It is noted that for a more accurate representation, we need to take into account the shape of the temperature distribution. We propose to employ an iterative approach where representative temperature distributions are computed with initial

isothermal cross sections that are then fed back to Serpent to create a more accurate cross section set.

We demonstrate that the developed SPH equivalence method can be applied to the three-dimensional HTR-PM model. We present a comparison of SPH-corrected MAMMOTH and Serpent calculations and find that they are in excellent agreement. In addition, we compute isothermal temperature coefficients of reactivity and control rod worth. The computed values are physically reasonable when compared with similar designs.

Coupled calculations are carried out using MAMMOTH-Pronghorn using SPH-corrected cross sections. For achieving convergence, the initial guess for the TH variables must be chosen judiciously, the full Jacobian must be assembled and then factorized using the *super lu* preconditioner. We qualitatively assess the eigenvalue, power distribution, solid and fluid temperature distributions, pressure, and vertical coolant speed. The obtained results do not exhibit any obvious unphysical features and the eigenvalue of the coupled calculation is in agreement with estimations based on the temperature coefficients of reactivity. It needs to be pointed out that in the absence of a reference solution, a quantitative assessment of the obtained results is impossible.

The presented portfolio of capabilities available in MAMMOTH-Pronghorn already exceeds existing capabilities in legacy codes significantly:

- MAMMOTH-Pronghorn can solve the N/TH problem in three-dimensional geometry while legacy codes cannot.
- MAMMOTH-Pronghorn can model conjugate heat transfer in strongly coupled calculations.
- MAMMOTH-Pronghorn can solve fully-transient problems, while the legacy codes only solve quasi-static problems.
- Pronghorn solves the TH problem in *r-z* geometry significantly faster than THERMIX-KONVEK because of its superior iterative methods. THERMIX-KONVEK wastes computational effort on converging a nested iteration scheme.
- MAMMOTH-Pronghorn's discretization method, FEM, features higher order of accuracy and hence requires significantly fewer elements for a desired level of accuracy than the legacy tools. The considered legacy tools limit the number of mesh elements which effectively limits the achievable accuracy.

- MAMMOTH-Pronghorn can take advantage of both multi-processor and multi-threading type parallelism allowing the solution of small, medium, and large problems. The considered legacy tools are limited to problems with at most 25,000 mesh elements. With 25,000 elements, THERMIX-KONVEK's execution time is of the order of several hours to half a day.
- MAMMOTH-Pronghorn is easily extendable because it is written in modern C++, while the legacy tools are written in Fortran77 and are not even actively maintained at this point.
- MAMMOTH-Pronghorn is well documented and follows NQA-1, while the legacy tools lack sufficient documentation.
- THERMIX-KONVEK's input is fixed format and does not allow comments. This shortcoming makes it difficult to keep input files well maintained and under quality control.

Additional work is required on MAMMOTH-Pronghorn to enhance efficiency and robustness. In particular, efficient pre-conditioning and careful parameter checking during the evaluation of correlations is recommended. Results for the three-dimensional HTR-PM model appear to be physical but a quantitative comparison to a credible benchmark calculation for a more physically accurate PBR model is recommended. Advanced modeling capabilities should be included in the analysis of more realistic PBR models to demonstrate their potential and application readiness.

We recommend the following tasks as future work:

- Further assessment of the LAMMPS DEM code for PBR analysis.
- Improved preconditioning.
- Automatic vetting of variables passed to correlations.
- Development of a more physically realistic PBR model following existing and published designs.
- Computation of temperature distributions across pebbles for more accurate cross section generation.
- TRISO temperature model especially for transients.

- Development of a credible reference solution for quantitative assessment of MAMMOTH-Pronghorn capabilities.
- Deployment of the Pebble Tracking Transport method and comparison with the homogenization approach.
- Assessment of capabilities for desired transient calculations.
- Assessment of the current radiation transfer capabilities in Rattlesnake.
- Use advanced modeling capabilities of Pronghorn including spatial dependent porosities and the modern equation system for creation of a more accurate PBR model.

References

[1] Zuoyi Zhang et al. "Current status and technical description of Chinese 2 x 250MWth HTR-PM demonstration plant". In: *Nuclear Engineering and Design* 239.7 (2009), pp. 1212–1219. ISSN: 0029-5493. DOI: https://doi.org/10.1016/j.nucengdes.2009.02.023. URL: http://www.sciencedirect.com/science/article/pii/S0029549309001332.

[2] H. Reutler. "Plant design and safety concept of the HTR-module". In: *Nuclear Engineering and Design* 109.1 (1988), pp. 335–340. ISSN: 0029-5493. DOI: https://doi.org/10.1016/0029-5493(88)90179-3. URL: http://www.sciencedirect.com/science/article/pii/0029549388901793.

[3] G.H. Lohnert. "The consequences of water ingress into the primary circuit of an HTR-Module - From design basis accident to hypothetical postulates". In: *Nuclear Engineering and Design* 134.2 (1992), pp. 159–176. ISSN: 0029-5493. DOI: https://doi.org/10.1016/0029-5493(92)90137-K. URL: http://www.sciencedirect.com/science/article/pii/002954939290137K.

[4] H.D. Gougar et al. *Pebbed6 - Theory Manual*. Unpublished INL report. 2018.

[5] H.D. Gougar et al. *Pebbed6 - User's Manual*. Unpublished INL report. 2018.

[6] H.D. Gougar and R.S. Sen. "On the Evaluation of Pebble Bed Reactor Critical Experiments Using the PEBBED Code". In: *Proceedings of the HTR 2014*. Weihai, China, 2014.

[7] E. Teuchert et al. *V.S.O.P ('94) Computer Code System for Reactor Physics and Fuel Cycle Simulation*. Research Report Jülich-2897. Forschungszentrum Jülich, 1994.

[8] W.Y. Yoon et al. *COMBINE7.0 - A Portable ENDF/B-VII.0 Based Neutron Spectrum and Cross-Section Generation Program*. Research Report INL/EXT-08-14729. Idaho Falls, ID: Idaho National Laboratory.

[9] R.J.J Stammler and M.J. Abbate. *Methods of Steady-State Reactor Physics in Nuclear Design*. Academic Press, 1983.

[10] R.E. MacFarlane and A.C. Kahler. "Methods for Processing ENDF/B-VII with NJOY". In: *Nuclear Data Sheets* 111.12 (2010). Nuclear Reaction Data, pp. 2739–2890. ISSN: 0090-3752. DOI: https://doi.org/10.1016/j.nds.2010.11.001. URL: http://www.sciencedirect.com/science/article/pii/S0090375210001006.

[11] M.G. Stamatelatos. "Rational Approximations for Cross-Section Space-Shielding in Doubly Heterogeneous Systems". In: *Nuclear Science and Engineering* 61.4 (1976), pp. 543–549.

[12] W.E. Engle. *A User's Manual for ANISN: A One-Dimensional Discrete Ordinates Transport Code with Anisotropic Scattering*. Tech. rep. K-1693. Oak Ridge Gaseous Diffusion Plant Computing Technology Center, 1967.

[13] S. Plimpton. "Fast Parallel Algorithms for Short-Range Molecular Dynamics". In: *J. Comp. Phys.* 117 (1995), pp. 1–19.

[14] *LAMMPS website*. https://lammps.sandia.gov/index.html. Accessed: 2018-11-27.

[15] Rimantas Kacianauskas et al. "Parallel discrete element simulation of poly-dispersed granular material". In: *Advances in Engineering Software* 41.1 (2010). Civil-Comp Special Issue, pp. 52–63. ISSN: 0965-9978. DOI: https://doi.org/10.1016/j.advengsoft.2008.12.004. URL: http://www.sciencedirect.com/science/article/pii/S0965997808002123.

[16] Chris H. Rycroft et al. "Granular flow in pebble-bed nuclear reactors: Scaling, dust generation, and stress". In: *Nuclear Engineering and Design* 265 (2013), pp. 69–84. ISSN: 0029-5493. DOI: https://doi.org/10.1016/j.nucengdes.2013.07.010. URL: http://www.sciencedirect.com/science/article/pii/S0029549313003427.

[17] J.Cogliati and A. Ougouag. *PEBBLES Operation and Theory Manual.* Tech. rep. INL/EXT-10-19305, r1. Idaho National Laboratory, 2010.

[18] J. Ortensi et al. *Benchmark Analysis of the HTR-10 with the MAMMOTH Reactor Physics Application*. Tech. rep. INL/EXT-18-45453. Idaho National Laboratory, 2018.

[19] J. Leppänen. "Development of a New Monte Carlo Reactor Physics Code". PhD thesis. Helsinki University of Technology, 2007.

[20] J. Ortensi et al. *Deterministic Modeling of the High Temperature Test Reactor*. Research Report INL/EXT-10-18969. Idaho Falls, ID: Idaho National Laboratory, 2010.

[21] J. Ortensi et al. *Methodologies and Requirements for the Generation of Physics Data Inputs to MAMMOTH Transient Simulations in Support of the Transient Reactor Test Facility*. Tech. rep. NL/LTD-15-36265. Idaho National Laboratory, Sept. 2015.

[22] J. Ortensi et al. *Updates to the Generation of Physics Data Inputs for MAMMOTH Simulations of the Transient Reactor Test Facility - FY2016*. Tech. rep. INL/EXT-16-39120. Idaho National Laboratory, June 2016.

[23] A. Novak et al. *Pronghorn Theory Manual*. Tech. rep. INL/EXT-18-44453. Idaho National Laboratory, 2018.

[24] L. Zou et al. “Stabilized finite element formulation for thermally-driven porous media flows in Pronghorn”. In: *ANS Annual Summer Meeting 2018, Driving the Future of Nuclear Technology*. ANS. Philadelphia, PA, 2018.

[25] H. Park et al. “Tightly Coupled Multiphysics Algorithms for Pebble Bed Reactors”. In: *Nuclear Science and Engineering* 166.2 (2010), pp. 118–133. DOI: 10.13182/NSE09-104. eprint: https://doi.org/10.13182/NSE09-104. URL: https://doi.org/10.13182/NSE09-104.

[26] Derek R. Gaston et al. “Physics-based multiscale coupling for full core nuclear reactor simulation”. In: *Annals of Nuclear Energy* 84 (2015), pp. 45–54. DOI: 10.1016/j.anucene.2014.09.060.

[27] Arif Masud and Thomas J.R. Hughes. “A stabilized mixed finite element method for Darcy flow”. In: *Computer Methods in Applied Mechanics and Engineering* 191.39 (2002), pp. 4341–4370. ISSN: 0045-7825. DOI: https://doi.org/10.1016/S0045-7825(02)00371-7. URL: http://www.sciencedirect.com/science/article/pii/S0045782502003717.

[28] Yaqi Wang, Sebastian Schunert, and Vincent Laboure. *Rattlesnake Theory Manual*. INL. 2017.

[29] Y. Wang. “Nonlinear Diffusion Acceleration for the Multigroup Transport Equation Discretized with SN and Continuous FEM With Rattlesnake”. In: *Proceedings to the International Conference on Mathematics, Computational Methods & Reactor Physics (M&C 2013)*. Sun Valley, Idaho, USA, May 2013.

[30] R.L. Williamson et al. “Multidimensional Multi-physics Simulation of Nuclear Fuel Behavior”. In: *Jou. Nucl. Mat.* 423.149–163 (2012).

[31] James J. Duderstadt and Louis J. Hamilton. *Nuclear Reactor Analysis*. New York: John Wiley & Sons, Inc., 1976.

[32] J. Morel. *A Non-Local Tensor Diffusion Theory*. Research Report LA-UR-07-5257. Los Alamos, NM: Los Alamos National Laboratory, 2007.

[33] T.J. Trahan and E.W. Larsen. “3-D ANISOTROPIC NEUTRON DIFFUSION IN OPTICALLY THICK MEDIA WITH OPTICALLY THIN CHANNELS”. In: *Proc. Int. Conf. on Mathematics and Computational Methods Applied in Nuclear Science and Engineering (MC 2011)*. ANS. Rio de Janeiro, Brazil, 2011.

[34] Z. Liu, K. Smith, and B. Forget. “A Cumulative migration method for computing rigorous transport cross sections and diffusion coefficients for LWR lattices with Monte Carlo”. In: *Physics of Reactors 2016 (PHYSOR 2016): Unifying Theory and Experiments in the 21st Century*. ANS. Sun Valley, ID, 2016.

[35] G. Mathonniere A. Hébert. “Development of a third generation superhomogenization method for the homogenization of pressurized water reactor assembly”. In: *Nuc. Sci. Eng.* 2 (1993), p. 115.

[36] J. Ortensi et al. “A Newton solution for the Superhomogenization method: The PJFNK-SPH”. In: *Annals of Nuclear Energy* 111 (Jan. 2018), pp. 579–594.

[37] Vincent Labouré et al. “Hybrid Super Homogenization and Discontinuity Factor Method for Continuous Finite Element Diffusion”. In: *Submitted to Annals of Nuclear Energy* (2018).

[38] Y. Wang et al. “A Pebble Tracking Transport Algorithm for Pebble Bed Reactor Analysis”. In: *PHYSOR 2018: Reactor Physics paving the way towards more efficient systems*. Cancun, Mexico, Apr. 2018.

[39] Vincent Laboure, Javier Ortensi, and Andrew Hummel. *HTTR 3-D Cross-Section Generation with Serpent and MAMMOTH*. Tech. rep. INL/EXT-18-51317. Idaho National Laboratory, 2018.

[40] Zuoyi Zhang et al. “The Shandong Shidao Bay 200 MWe High-Temperature Gas-Cooled Reactor Pebble-Bed Module (HTR-PM) Demonstration Power Plant: An Engineering and Technological Innovation”. In: *Engineering* 2 (Mar. 2016), pp. 112–118. DOI: 10.1016/J.ENG.2016.01.020.

[41] *Evaluation of high temperature gas cooled reactor performance:Benchmark analysis related to initial testing of the HTTR and HTR-10.* Tech. rep. IAEA-TECDOC-1382. International Reactor Physics Experiment Evaluation Project, 2003.

[42] *Evaluation of the Initial Critical Configuration of the HTR-10 Pebble-bed reactor.* Tech. rep. HTR10-GCR-RESR-001. International Reactor Physics Experiment Evaluation Project, 2006.

[43] Kurt Kugeler and Zuoyi Zhang. *Modular High-temperature Gas-cooled Reactor Power Plant*. Berlin Heidelberg: Springer-Verlag, 2019. ISBN: 978-3-662-57710-3.

[44] Jingyu Zhang, Fu Li, and Yuliang Sun. “Physical Analysis of the Initial Core and Running-In Phase for Pebble-Bed Reactor HTR-PM”. In: *Science and Technology of Nuclear Installations* 8918424 (2017).

[45] L Massimo. *Physics of High-Temperature Reactors*. New York: Pergamon Press, 1976. ISBN: 978-1-483-28028-8.

[46] J. I. Duo and Y. Y. Azmy. "Spatial Convergence Study of Discrete Ordinates Methods Via the Singular Characteristic Tracking Algorithm". In: *Nuclear Science and Engineering* 162.1 (2009), pp. 41–55. DOI: 10.13182/NSE08-28. eprint: https://doi.org/10.13182/NSE08-28. URL: https://doi.org/10.13182/NSE08-28.

[47] G. van Heerden, S. Sen, and F. Reitsma. "Calculational Approach and Results of the Safe Shutdown Earthquake Event for the Pebble Bed Modular Reactor". In: *Proceedings of PHYSOR 2006*. Canadian Nuclear Society. Vancouver, BC, 2006.

[48] K.A. Klein-Tebbe. *SAMSON - A Vibration Test Facility for Simulating Multi-Axis Dynamic Motion*. Tech. rep. D HRB 1229 85 E. Brown Bovari HRB internal document, 1985.

[49] R.F. Benenati and C.B. Brosilow. "Void Fraction Distribution in Beds of Spheres". In: *AIChE Journal* 8.3 (1962), p. 359.

[50] G.D. Scott and D.M. Kilgour. "The density of random close packing of spheres". In: *Journal of Physics D: Applied Physics* 2 (1969), p. 863.

[51] J.T. Cox. "The Modeling of Core-Wide Behavior of Pebble Bed Reactors Using Static and Dynamic Graphite Pebble Properties to Predict Core Performance and Safety Behavior". PhD thesis. Oregon State University, 2018.

[52] C. Kloss et al. "Models, algorithms and validation for open-source DEM and CFD-DEM". In: *Progress in Computational Fluid Dynamics* 12 (2012), pp. 140–152.

[53] Alexander Stukowski. "Visualization and analysis of atomistic simulation data with OVITO-the Open Visualization Tool". In: *Modelling and Simulation in Materials Science and Engineering* 18.1 (2010), p. 015012. URL: http://stacks.iop.org/0965-0393/18/i=1/a=015012.

[54] G.H. Lohnert. "Technical design features and essential safety-related properties of the HTR-Module". In: *Nuclear Engineering and Design* 121.2 (1990), pp. 259–275. DOI: 10.1016/0029-5493(90)90111-A. URL: https://www.sciencedirect.com/science/article/pii/002954939090111A.

[55] J. Ortensi. "An Earthquake Transient Method for Pebble-Bed Reactors and a Fuel Temperature Model for TRISO Fueled Reactors". PhD thesis. Idaho State University, 2009.

[56] J. Mayer and N. Hottle et. al. *Pebble Bed Reactor Technology Readiness Study*. Tech. rep. 12-9151714-000. Areva Np Inc., 2018.